International Journal of Heat and Mass Transfer 51 (2008) 6136–6156

Contents lists available at ScienceDirect

International Journal of Heat and Mass Transfer

journal homepage: www.elsevier.com/locate/ijhmt

Theoretical analysis on microwave heating of oil–water emulsions supported on ceramic, metallic or composite plates

Sujoy Kumar Samanta [a], Tanmay Basak [a,b], Bhaskar Sengupta [b,*]

[a] Department of Chemical Engineering, Indian Institute of Technology Madras, Chennai 600036, India
[b] School of Planning, Architecture and Civil Engineering, Queen's University Belfast, David Keir Building, Stranmillis Road, Belfast BT9 5AG Northern Ireland, UK

ARTICLE INFO

Article history:
Received 25 July 2007
Available online 2 June 2008

Keywords:
Microwave
Oil–water emulsion
Composite supports
Thermal runaway

ABSTRACT

A detailed theoretical analysis has been carried out to study efficient heating due to microwaves for one-dimensional (1D) oil–water emulsion samples placed on various ceramic, metallic (reflective) and ceramic–metallic composite supports. Two typical emulsion systems are considered such as oil-in-water (o/w) and water-in-oil (w/o). A preliminary study has been carried out via average power vs emulsion thickness diagram to estimate microwave power absorption within emulsion samples for various cases. The maxima in average power, also termed as 'resonances', are observed for specific emulsion thicknesses and the two consecutive resonances of significant magnitudes are termed as R_1 and R_2 modes. For both o/w and w/o emulsions, it is observed that microwave power absorption is enhanced in presence of metallic and composite supports during both R_1 and R_2 modes. The efficient heating strategies characterized by 'large heating rates' with 'minimal thermal runaway' i.e. uniform temperature distributions within the sample have been assessed for each type of emulsion. Based on the detailed spatial distributions of power and temperature for various cases, SiC-metallic composite support may be recommended as an optimal heating strategy for o/w samples with higher oil fractions ($\phi \geqslant 0.45$) whereas metallic and Alumina-metallic composite supports may be favored for samples with smaller oil fractions ($\phi = 0.3$) during R_1 mode. For w/o samples, SiC-metallic composite support may be suitable heating strategy for all ranges of water fractions during R_1 mode. During R_2 mode, metallic and Alumina-metallic composite supports are favored for both o/w and w/o emulsion samples. Current study recommends the efficient way to use microwaves in a single mode waveguide and the heating strategy can be suitably extended for heating of any other emulsions for which dielectric properties are easily measurable or available in the literature.

1. Introduction

Electromagnetic radiations in the frequency range 300 MHz to 300 GHz are known as microwaves. During microwave heating, the material dielectric loss which is a function of frequency of microwaves causes electrical energy to convert into heat within material and this involves the mechanism termed as 'volumetric heating' which is responsible to carry out uniform and faster processing of materials. Microwave energy has largely been used for thermal processing in a wide range of food and chemical process industries for pasteurizing, heating, drying, petroleum refining, sintering of ceramics, and many others [1–15]. Oil–water emulsion heating is a very common industrial practice in petroleum refining as about 80% of exploited crude oils exist in the form of emulsion [13]. Various oil-in-water (o/w) and water-in-oil (w/o) emulsions also occur in other industrial operations, such as oil and gas production, food processing industries, which include dressings, sauces, butter, mayonnaise, and many more. Efficient heating of emulsions is required for a faster processing based on industrial demand and microwave heating has largely been used due to its 'volumetric heating' effects.

Enhanced power absorption and large volumetric heating effects occur for samples with specific dimensions in presence of 'resonances' of microwave power. A number of theoretical and experimental investigations were carried out by earlier researchers on various aspects of microwave heating, especially on resonances. Ayappa et al. [16–18] carried out theoretical and numerical studies on microwave heating of 1D slabs and 2D cylinders. Further, Ayappa et al. [19] and Ayappa [20] analyzed resonances occurring only for fixed sample dimensions of 1D slabs and 2D cylinders. They also established suitable relationships on occurrence of resonance with sample size. Microwave heating and transport models were further applied for thawing and heating of multiphase systems

* Corresponding author.
E-mail addresses: sujoysamanta@smail.iitm.ac.in (S.K. Samanta), tanmay@iitm.ac.in (T. Basak), B.Sengupta@qub.ac.uk (B. Sengupta).

0017-9310/$ - see front matter Crown copyright © 2008 Published by Elsevier Ltd. All rights reserved.
doi:10.1016/j.ijheatmasstransfer.2008.04.003

Nomenclature

$A_{x,l}$	amplitude of stationary wave for lth layer, V m^{-1}
c_p	specific heat capacity, J kg^{-1} K^{-1}
c	velocity of light, m s^{-1}
E_x	electric field intensity, V m^{-1}
f	frequency, Hz
h	heat transfer coefficient, W m^{-2} K^{-1}
H_y	magnetic field intensity, A m^{-1}
k	thermal conductivity, W m^{-1} K^{-1}
L	half-slab thickness, m
L_s	sample thickness, m
q	microwave source term, W m^{-3}
t	time, s
T	temperature, K
z	distance, m

Greek symbols

ϵ_0	free space permittivity, Farad m^{-1}
κ	propagation constant
κ'	relative dielectric constant
κ''	relative dielectric loss
κ^*	relative complex dielectric properties
ρ	density, kg m^{-3}
ϕ	fraction of the dispersed phase (–)
$\delta_{x,l}$	phase difference in stationary wave for lth layer
ω	angular frequency, Rad s^{-1}

Subscripts

c	continuous phase
d	dispersed phase
eff	effective property
l	layer number

Superscripts

t	transmitted wave
r	reflected wave

[21–26] and greater rates in material processing were achieved due to resonances. Although microwave heating in presence of resonances accelerates the processing rates, the local thermal runaway or overheating may occur within the sample. The local thermal runaway associated with resonances was also observed for heating of materials supported on various ceramic plates [27]. All these studies are limited within microwave heating of simple systems where complex dielectric interaction was absent for predictions of heating rates.

To date, a few studies are based on microwave heating and processing of multiphase systems, especially emulsions. Emulsion consists of a continuous phase and a dispersed phase and based on the nature of continuous medium, two typical emulsions are considered as oil-in-water (o/w) and water-in-oil (w/o). A few earlier studies on microwave heating of oil–water emulsions were carried out for several applications such as measurement of dielectric properties of oil–water emulsions [28,29], heating of oil–water emulsions [25,26], and demulsification of water-in-oil emulsions [11,12]. Pal [28] reported a comprehensive review of the available techniques on measurement of the oil and water content of emulsions and effective dielectric properties of oil–water emulsions. Later, Erle et al. [29] also studied dielectric properties of o/w and w/o emulsions measured at a frequency of 2.45 GHz by an open-ended coaxial-line probe. They proposed correlations for the effective dielectric properties of oil–water emulsions and their correlations show well agreement with the experimental results.

An earlier theoretical and experimental investigation on microwave heating of oil–water emulsion systems was carried out by Barringer et al. [25]. They carried out experimental studies for various oil–water fractions with fixed beaker radii in a microwave oven. Based on the experimental observations they found resonance (maxima in average power) occurring only for fixed sample dimensions. Fang and Lai [11] and Chan and Chen [12] carried out experimental studies on the conditions of demulsification, especially on water-in-oil emulsions. Basak [26] carried out preliminary theoretical analysis on enhanced heating of oil–water emulsions (o/w and w/o) for specific emulsion contents in absence of any support. A detailed analysis on microwave heating of emulsions in presence of various ceramic and/or metallic plates may be important for studying efficient heating process which may be useful for industrial processing. Microwave heating of emulsion in presence of various ceramic–metallic composite supports may be non-trivial due to complex interaction between emulsions (o/w and w/o) and supports. In addition, ceramic–metallic composite support assembly may pose some interesting issues on optimal thermal runaway for systems involving multiple interfaces, which were overlooked by earlier researchers. Efficient heating strategies for emulsion-support assembly where support may consist of ceramic and/or metallic plates will find direct application in chemical process industries (CPI), especially in petroleum refineries and these studies are yet to appear in literature.

Current studies attempt to carry out a detailed theoretical investigation on microwave processing of oil–water emulsions supported on ceramic and/or metallic plates. We have modeled the effective dielectric response of the oil–water emulsions (both o/w and w/o) based on the study of Erle et al. [29] and their correlation [29] is suitable for the current investigation with the frequency of 2.45 GHz at which domestic microwave ovens operate. Maxwell's equations and the non-linear heat conduction equation are simultaneously solved using Galerkin's finite element method to obtain power absorption and transient temperature profile for the emulsion and support. A detailed analysis has been carried out for 'resonances' or maxima in microwave power absorption during heating of o/w and w/o emulsions with various fractions of the dispersed phase. During resonances, an emulsion absorbs greater power and the presence of a support may alter power absorption within an emulsion. The resonating phenomena is quite complex for an emulsion-support composite and a preliminary study has been carried out on the resonances to estimate power absorption for such emulsion-support composites. The role of individual traveling waves on spatial power and temperature distributions within the emulsion sample and support has also been analyzed. The efficient heating strategies characterized by 'large heating rates' with 'minimal thermal runaway effects' within the sample have been assessed for each type of emulsion. Optimal strategies for thermal processing of emulsion-support composites have been recommended based on several case studies for both o/w and w/o emulsions.

2. Theory

2.1. Electric field and power evaluations in multilayered and multiphase system

Consider a multilayered slab of thickness 2L exposed to microwaves as shown in Fig. 1. We will investigate the heating charac-

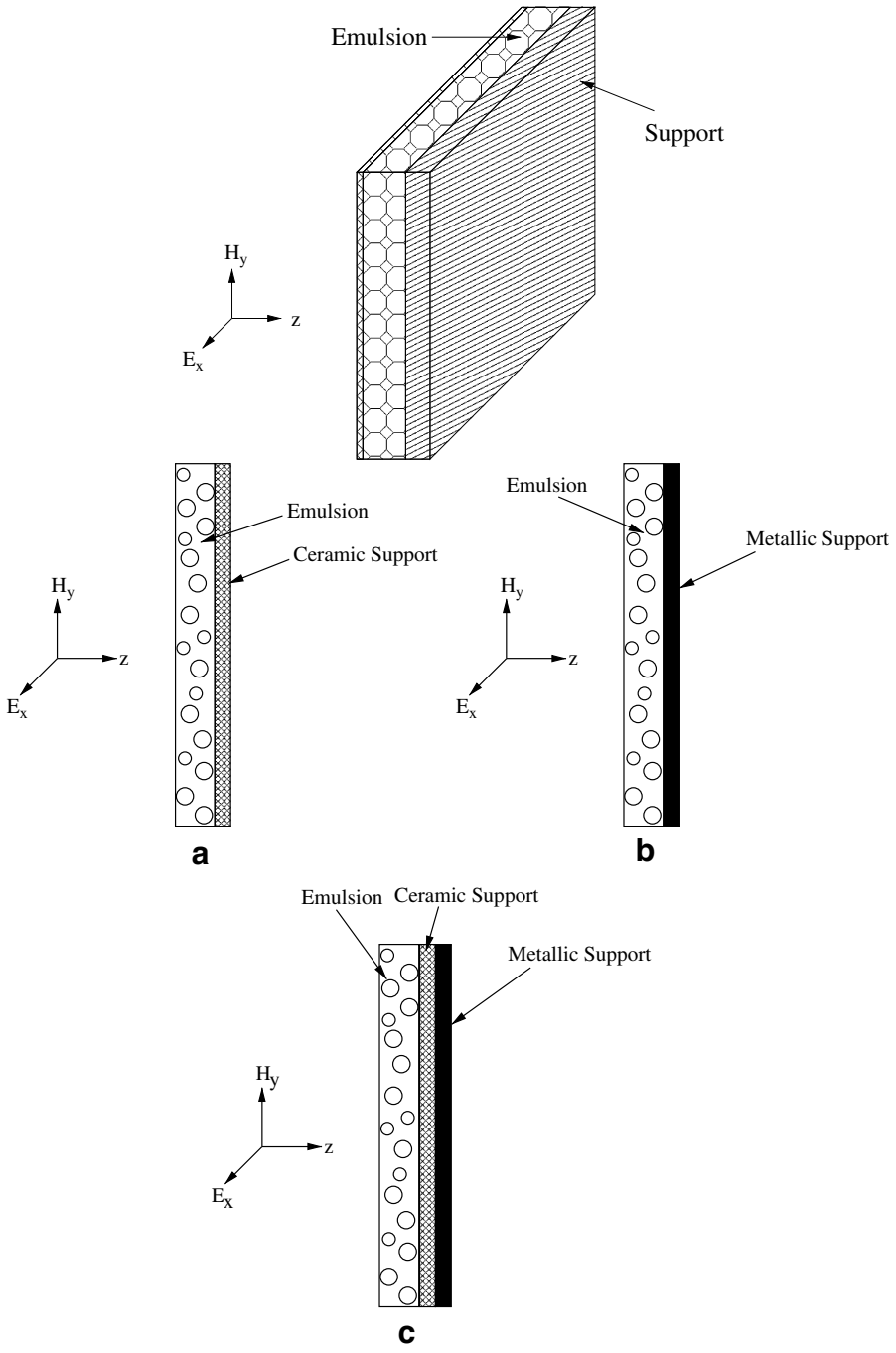

Fig. 1. Schematic illustration of a sample with single/composite support exposed to a plane electromagnetic wave.

teristics of emulsion samples either on metallic or ceramic or ceramic–metallic composite support as shown in Fig. 1. The electromagnetic wave propagation due to uniform electric field E_x, given by Maxwell's equation is

$$\frac{d^2E_x}{dz^2} + \kappa^2 E_x = 0, \tag{1}$$

where E_x lies in x–y plane and varies only in the direction of propagation, z axis (Fig. 1). In Eq. (1), $\kappa = \frac{\omega}{c}\sqrt{\kappa' + i\kappa''}$ is the propagation constant which depends on the dielectric constant, κ' and the dielectric loss, κ''. It may be noted that, $\omega = 2\pi f$, where f is the frequency of the electromagnetic wave and c is the velocity of light. In a n multilayered sample the electric field for the lth layer obtained from Eq. (1) is

$$\frac{d^2E_{x,l}}{dz^2} + \kappa_l^2 E_{x,l} = 0, \tag{2}$$

where $z_{l-1} \leqslant z \leqslant z_l$ and $l = 1 \ldots n$. Here z_l denotes the coordinate of the phase interface between lth and $(l+1)$th layers. Note that, $l = 1$ denotes air layer, $l = 2$ denotes emulsion layer and the ceramic/metallic support may be denoted as $l = 3, 4, \ldots$. We assume that the dielectric properties are independent of temperature and constant in each layer. Hence, the general solution to Eq. (2) represented as a linear combination of transmitted and reflected waves propagating in opposite directions is

$$E_{x,1} = E_{t,1}e^{i\kappa_1 z} + E_{r,1}e^{-i\kappa_1 z}, \quad z \leqslant z_1,$$
$$E_{x,l} = E_{t,l}e^{i\kappa_l z} + E_{r,l}e^{-i\kappa_l z}, \quad z_{l-1} \leqslant z \leqslant z_l,$$
$$E_{x,n} = \begin{cases} E_{t,n}e^{i\kappa_n z} + E_{r,n}e^{-i\kappa_n z}, & z = z_n \quad \text{(air)}, \\ 0, & z = z_n \quad \text{(metallic support)}, \end{cases} \tag{3}$$

where $E_{t,l}$ and $E_{r,l}$ are the coefficients due to transmission and reflection, respectively. The boundary conditions at the interface are

$$\left.\begin{aligned} E_{x,l-1} &= E_{x,l} \\ \tfrac{dE_{x,l-1}}{dz} &= \tfrac{dE_{x,l}}{dz} \end{aligned}\right\} \begin{aligned} l &= 2 \ldots n \\ z &= z_1 \ldots z_{n-1}. \end{aligned} \tag{4}$$

The interface conditions Eq. (4) and the general solutions Eq. (3), are used to obtain the coefficients, $E_{t,l}$ and $E_{r,l}$ via solving the set of algebraic equations:

$$\left.\begin{aligned} &E_{t,l}e^{i\kappa_l z_l} + E_{r,l}e^{-i\kappa_l z_l} - E_{t,l+1}e^{i\kappa_{l+1} z_l} - E_{r,l+1}e^{-i\kappa_{l+1} z_l} = 0 \\ &\kappa_l E_{t,l}e^{i\kappa_l z_l} - \kappa_l E_{r,l}e^{-i\kappa_l z_l} - \kappa_{l+1}E_{t,l+1}e^{i\kappa_{l+1} z_l} \\ &\quad + \kappa_{l+1}E_{r,l+1}e^{-i\kappa_{l+1} z_l} = 0 \end{aligned}\right\} l = 1 \ldots n-1. \tag{5}$$

The electric field intensities at the first and last mediums are known, i.e. $E_{t,1} = E_0$ and $E_{r,n} = 0$ (for air) and $E_{t,n} = E_{r,n} = 0$ (for metallic support). The incident field at the left face E_0 can be obtained from the intensity of microwave source, I_0 as

$$E_0 = \sqrt{\frac{2I_0}{c\epsilon_0}}. \tag{6}$$

Eq. (5) are solved for the remaining $2n-2$ coefficients using OCTAVE/MATLAB [24,26,27]. For the lth layer, the transmitted and reflected waves are

$$E^t_{x,l} = E_{t,l}e^{i\kappa_l z} = A^t_{x,l}e^{i\delta^t_{x,l}},$$
$$E^r_{x,l} = E_{r,l}e^{-i\kappa_l z} = A^r_{x,l}e^{i\delta^r_{x,l}}, \tag{7}$$

where corresponding amplitudes are given by

$$A^t_{x,l} = \sqrt{E^t_{x,l}E^{t\,*}_{x,l}}$$
$$A^r_{x,l} = \sqrt{E^r_{x,l}E^{r\,*}_{x,l}} \tag{8}$$

and the phase states are given by

$$\delta^t_{x,l} = \tan^{-1}\left[\frac{\mathrm{Im}(E^t_{x,l})}{\mathrm{Re}(E^t_{x,l})}\right],$$
$$\delta^r_{x,l} = \tan^{-1}\left[\frac{\mathrm{Im}(E^r_{x,l})}{\mathrm{Re}(E^r_{x,l})}\right], \tag{9}$$

where the superscript, '*' in Eq. (8) denotes the complex conjugate. For a stationary wave in the lth layer, the amplitude is given by

$$A_{x,l} = \sqrt{E_{x,l}E^*_{x,l}} \tag{10}$$

and the difference in phase angle is given by

$$\delta_{x,l} = \delta^t_{x,l} - \delta^r_{x,l}, \tag{11}$$

where the quantities $E_{x,l}$ and $E^*_{x,l}$ appeared in Eq. (10) are evaluated using Eqs. (3) and (7). At the resonance, the difference in phase angle is zero, i.e., $\delta_{x,l} = 0$.

The absorbed power in lth layer, obtained from Poynting vector theorem is

$$q_l(z) = \frac{1}{2}\omega\epsilon_0\kappa''_{\mathrm{eff}}(\phi)E_{x,l}(z)E^*_{x,l}(z). \tag{12}$$

Here ϵ_0 is the free space permittivity, ϕ is the volume fraction of the dispersed phase and κ''_{eff} is the effective dielectric loss where

$$\kappa^*_{\mathrm{eff}}(\phi) = \kappa'_{\mathrm{eff}}(\phi) + i\kappa''_{\mathrm{eff}}(\phi). \tag{13}$$

For o/w emulsion, the effective dielectric property (κ^*_{eff}) is [29]

$$\kappa^*_{\mathrm{eff}} = \frac{\kappa^*_c[\kappa^*_d(1+a\phi) + a\kappa^*_c(1-\phi)]}{\kappa^*_d(1-\phi) + \kappa^*_c(a+\phi)}. \tag{14}$$

Here κ^*_c and κ^*_d are the relative complex dielectric properties of the continuous (water) and dispersed (oil) phases, respectively; $a = 2$ for spherical dispersions and $a = 1$ for cylindrical dispersions. Based on the experimental observations, $a = 1$ is chosen for o/w emulsion study [29]. Experimental data on effective dielectric properties of w/o emulsions were best fitted by Lichtenecker and Rother as reported by Erle et al. [29] and effective dielectric properties are obtained as

$$\ln\kappa^*_{\mathrm{eff}} = \phi\ln\kappa^*_d + (1-\phi)\ln\kappa^*_c. \tag{15}$$

The average power obtained by integrating the power across the slab is

$$\bar{q} = \frac{1}{2L}\int_{-L}^{+L} q_l(z)\,dz \approx \frac{1}{n}\sum_{i=1}^{n} q_l(z_i). \tag{16}$$

Here $-L$ and L denote the left and right faces of the slab, respectively and $q_l(z)$ denotes the power as a function of z where z may be measured from the left edge of the slab or sample. Note that, $2L$ is the thickness of the entire slab consisting of emulsion sample and supports. We will denote L_s as the thickness of the emulsion sample and L' as the total thickness of the supports such that $2L = L_s + L'$. The average power for a sample of thickness L_s is

$$q_{\mathrm{av}} = \frac{1}{n}\sum_{i=1}^{n} q_l(z_i), \quad \text{for } 0 \leqslant z_i \leqslant L_s. \tag{17}$$

It may be noted that, the effective power absorption (q_{eff}) within an emulsion sample of thickness L_s may be obtained as

$$q_{\mathrm{eff}} = q_{\mathrm{av}}L_s, \tag{18}$$

where unit cross-section of the sample has been assumed.

2.2. Modeling of microwave heating

The energy balance equation due to microwave assisted heat source is

$$\rho c_p\frac{\partial T}{\partial t} = k\frac{\partial^2 T}{\partial z^2} + q(z), \tag{19}$$

where ρ, the effective density, c_p, the effective specific heat and k, the effective thermal conductivity may be expressed as effective property such that

$$\rho = (1-\phi)\rho_c + \phi\rho_d \tag{20}$$
$$c_p = (1-\phi)c_{p_c} + \phi c_{p_d} \tag{21}$$

and

$$k = (1-\phi)k_c + \phi k_d. \tag{22}$$

It may be noted that the density, ρ in Eq. (20) is the effective density. An uniform bulk density throughout the emulsion is assumed as difference in density between oil and water phase is very small and the natural convection within the sample is neglected.

The volumetric heat source, in Eq. (19), $q(z)$ is defined in a similar manner as in Eq. (12). In a n multilayered sample, the energy balance equation for the lth layer obtained from Eq. (19) is

Table 1
The thermal and dielectric properties are given for water, oil, Al_2O_3 and SiC [26,27,14]

Material property	Water	Oil	Al_2O_3	SiC
Heat capacity, C_p (J kg^{-1} K^{-1})	4190	2000	1046	3300
Thermal conductivity, k (W m^{-1} K^{-1})	0.609	0.168	26	40
Density, ρ (kg m^{-3})	1000	900	3750	3100
Dielectric constant (2450 MHz), κ'	78.1	2.8	10.8	26.66
Dielectric loss (2450 MHz), κ''	10.44	0.15	0.1566	27.99

$$(\rho c_p)_l \frac{\partial T_l}{\partial t} = k_l \frac{\partial^2 T_l}{\partial z^2} + q_l(z) \quad l = 1 \ldots n. \tag{23}$$

The boundary conditions are

$$\frac{\partial T_1}{\partial z} = 0 \quad z = z_1 \tag{24}$$

and

$$\frac{\partial T_{n-1}}{\partial z} = 0 \quad z = z_{n-1}. \tag{25}$$

The boundary condition Eq. (24) has been assumed for the interface between air and the sample due to following objectives: (1) heating effects are solely due to the heat generation and (2) the entire microwave heating process is carried out with insulated situation at end points and hence, heat loss to the ambiance is neglected. The boundary condition Eq. (25) at the right end of ceramic/metallic or composite support has been assumed to represent insulated condition. Individual ceramic support is covered by insulated materials whereas the thin metallic supports are assumed to surround insulated materials and therefore within metallic supports no flux condition is still valid.

The interface conditions between ceramic and material are

$$\left.\begin{aligned} T_l &= T_{l+1} \\ k_l \tfrac{\partial T_l}{\partial z} &= k_{l+1} \tfrac{\partial T_{l+1}}{\partial z} \end{aligned}\right\} \begin{aligned} &l = 2 \ldots n-2 \\ &z = z_2 \ldots z_{n-2}. \end{aligned} \tag{26}$$

It may be noted that the electric field (see wave propagation equation, Eq. (2)) is a complex quantity. Therefore, the closed form solution of electric field Eq. (2) within a sample with various support assemblies may be cumbersome. Alternatively, the complex electric field can be viewed as a combination of real and imaginary parts. Hence, Eq. (2) reduces to two coupled differential equations for real and imaginary parts. In addition, boundary conditions of differential equations for electric fields are also coupled and they are Robin non-homogeneous types. Therefore, the coupled differential equations are solved numerically. The numerical solutions of electric field have further been supplemented in heat generation term ($q_l(z)$) of energy balance equation Eq. (23) which also has been solved numerically. Dimensionless forms of governing equations and boundary conditions are discussed next.

2.3. Dimensionless analysis

Note that, $z' = \frac{z+L}{2L}$ as $-L \leqslant z \leqslant L$. Using dimensionless variables

$$u = \frac{E_{x,l}}{E_0} \quad \text{and} \quad \frac{\mathrm{d}}{\mathrm{d}z'} = 2L\frac{\mathrm{d}}{\mathrm{d}z}.$$

Eq. (2) reduces to

$$\frac{\mathrm{d}^2 u}{\mathrm{d}z'^2} + \gamma^2 u = 0, \tag{27}$$

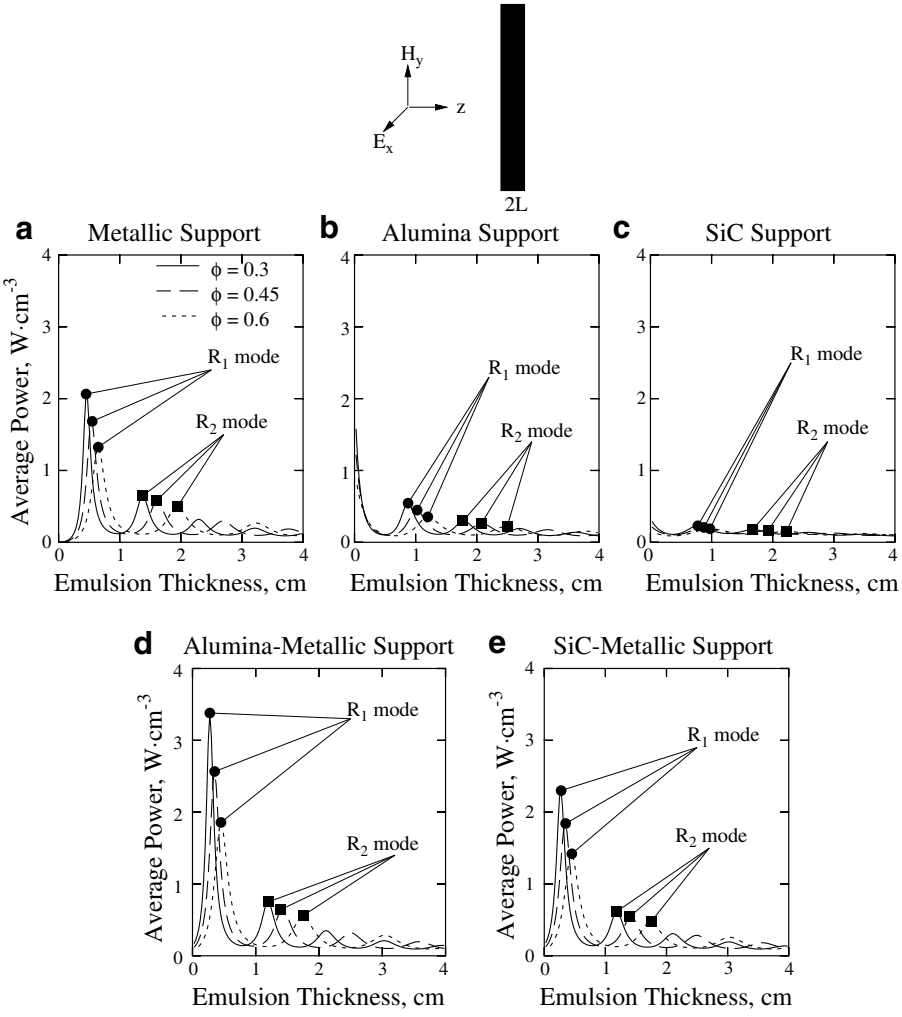

Fig. 2. Average power (W cm^{-3}) vs emulsion thickness (cm) for various oil-in-water (o/w) emulsion samples with (a) metallic support, (b) alumina support, (c) SiC support, (d) alumina-metallic support and (e) SiC-metallic support. The symbol, •, denotes R_1 mode and the symbol, ■, denotes R_2 mode of resonances.

where u is the electric field intensity, $\gamma = \frac{2L\omega}{c}\sqrt{\kappa' + i\kappa''}$ is the propagation constant and $2L$ is the thickness of the slab. Substituting the complex field variable $u = v + iw$ into Eq. (27) and equating the real and imaginary components, we get

$$\frac{d^2v}{dz'^2} + \chi_1 v - \chi_2 w = 0 \tag{28}$$

and

$$\frac{d^2w}{dz'^2} + \chi_2 v + \chi_1 w = 0, \tag{29}$$

with $\chi_1 = \frac{4L^2\omega^2}{c^2}\kappa'$ and $\chi_2 = \frac{4L^2\omega^2}{c^2}\kappa''$. The boundary conditions for the real and imaginary components are [17]

$$\left.\begin{array}{l} \frac{dv}{dz'} - \frac{2\omega L}{c} w = \frac{4\omega L}{c}\sin\left(\frac{\omega L}{c}\right) \\ \frac{dw}{dz'} + \frac{2\omega L}{c} v = \frac{4\omega L}{c}\cos\left(\frac{\omega L}{c}\right) \end{array}\right\} \quad \text{at} \quad z' = 0 \tag{30}$$

and

$$\left.\begin{array}{l} \frac{dv}{dz'} + \frac{2\omega L}{c} w = 0 \\ \frac{dw}{dz'} - \frac{2\omega L}{c} v = 0 \end{array}\right\} \quad \text{at} \quad z' = 1. \tag{31}$$

Dimensionless form of the energy balance equation in presence of microwave, Eq. (23), is

$$(\overline{\rho c_p})_l \frac{\partial \theta_l}{\partial \tau} = \bar{k}_l \frac{\partial^2 \theta_l}{\partial z'^2} + Q_l(z'), \tag{32}$$

where

$$\theta_l = \frac{T_l - T_\infty}{T_0}, \quad (\overline{\rho\ c_p})_l = \frac{(\rho c_p)_l}{\rho_0 c_{p0}} \quad \text{and} \quad \bar{k}_l = \frac{k_l}{k_0}.$$

The expression for the microwave power term in Eq. (32) is

$$Q_l(z') = \frac{2L^2\omega\epsilon_0\kappa'' E_0^2}{k_0 T_0}(v^2 + w^2). \tag{33}$$

The boundary conditions in dimensionless form, Eqs. (24) and (25) are

$$\frac{\partial \theta_1}{\partial z'} = 0, \quad z' = 0 \tag{34}$$

and

$$\frac{\partial \theta_{n-1}}{\partial z'} = 0, \quad z' = 1. \tag{35}$$

The initial condition used in the analysis is

$$\theta(\tau = 0) = \frac{T_0 - T_\infty}{T_0}, \quad \text{for} \quad 0 \leqslant z' \leqslant 1. \tag{36}$$

It may be noted that, the coupled differential equations Eqs. (28) and (29) are associated with the coupled non-homogeneous Robin boundary conditions Eqs. (30) and (31). Eqs. (28) and (29) have been solved using Galerkin Finite Element method [30]. The motivation of solution procedure in Galerkin weak form is due to fact that the non-homogeneous coupled Robin boundary condi-

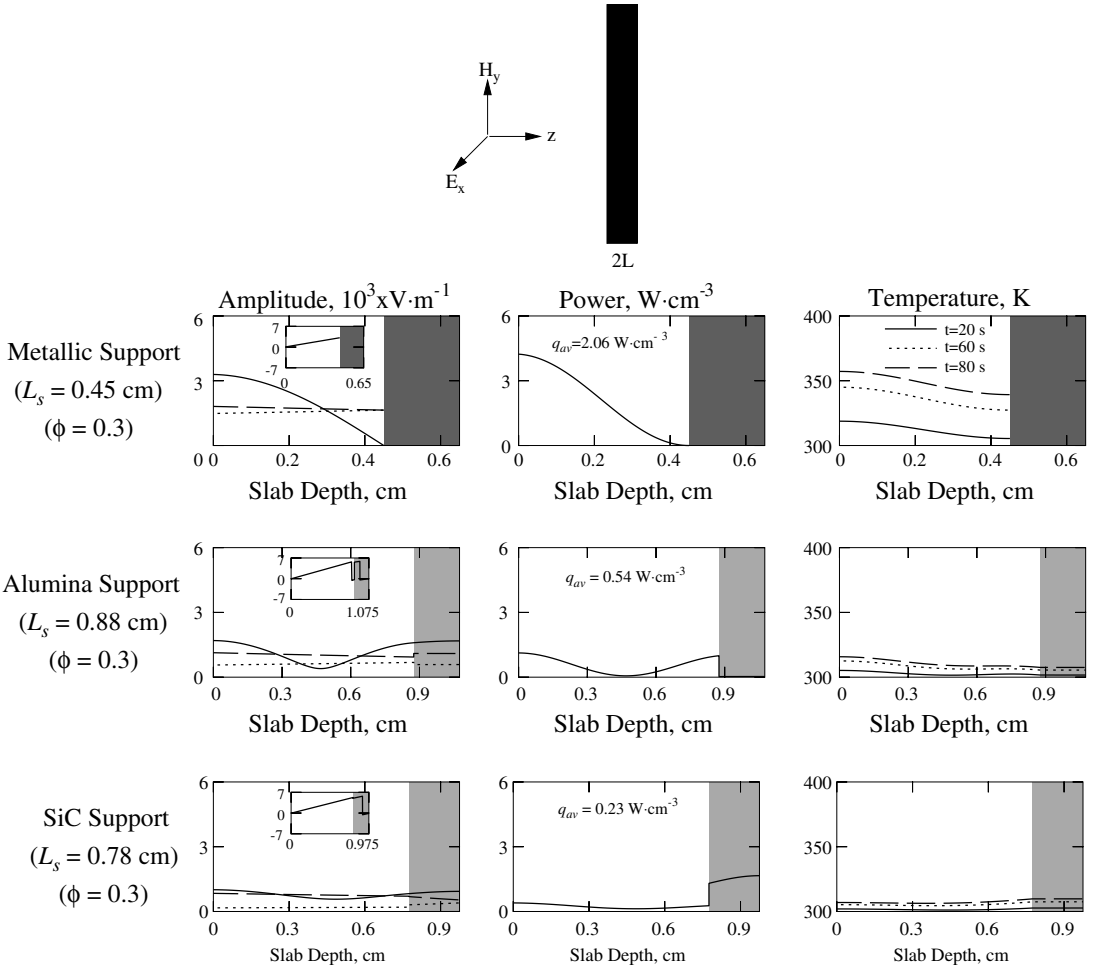

Fig. 3. Amplitudes of electric field ($A_{x,l}, A^t_{x,l}, A^r_{x,l}$), power distributions and temperature profiles for 30% oil-in-water (o/w) emulsion samples with metallic support, Alumina support and SiC support during R_1 mode. The support thickness= 0.2 cm. — —, transmitted wave; . . ., reflected wave; —·—, stationary wave. The light and dark shaded regimes denote ceramic and metallic support, respectively. The inset shows phase difference ($\delta_{x,l}$) vs z.

tions can be included automatically in boundary integrals of residuals as discussed in earlier references [30,17]. The electric field solutions are further employed for solving energy balance equation via finite element method with identical basis functions for electric fields and temperatures. In addition, for various interfaces with support, the interface element automatically satisfies flux continuity and field variable continuity as discussed by Reddy [30] and Ayappa et al. [17].

To discretize the time domain, Crank–Nicholson method is used, and residual equations are solved using Newton Raphson Method [17,21,24]. Due to the lack of a good initial guess to begin the Newton scheme, a small time step $\Delta t = 1 \times 10^{-4}$ s was used at the first time step. Unless specified otherwise $\Delta t = 0.1$ s was used for subsequent steps. Note that, typically 30–60 elements for the whole emulsion-support assembly (10–20 elements for supports and 20–40 elements for sample) were used. It was found that the maximum difference between the values of the unknowns at the nodes was less than 1% when the values were compared for 30 and 60 elements. Similarly, the maximum difference was less than 1% when the results were compared for $\Delta t = 0.05$ s and 0.1 s.

The dielectric and thermal properties are obtained from Table 1. Note that, the dielectric properties correspond to a microwave frequency of 2450 MHz. In all cases, the sample is exposed to the microwave radiation of intensity 1 W cm^{-2} and the insulated boundary condition has been assumed at the outer faces of the assembly. The temperature of the emulsion and the support is maintained at 300 K at $t = 0$ s. The typical oil–water emulsion systems are considered as oil-in-water (o/w) and water-in-oil (w/o) emulsions with various fractions (ϕ) of the dispersed phase. We have considered three ϕ values for both the emulsion (o/w and w/o) samples as 0.3, 0.45 and 0.6. We will illustrate the role of ceramic, metallic and ceramic–metallic composites on microwave power and thermal characteristics for various cases in presence of 'resonances'. The thickness of the sample varies between few mm to few cm and we have assumed the thickness of the ceramic support to be 0.2 cm for all test cases. Note that, Al_2O_3 is a transparent medium [14], SiC absorbs microwave significantly [14] and metallic support reflects microwave completely. Therefore, we have assumed smaller thickness of support and the influence of various thicknesses of support on microwave heating of emulsions may not be important for current work.

3. Results and discussion

3.1. Microwave power and temperature distributions for oil-in-water (o/w) emulsions

A detailed analysis has been carried out to study the role of metallic (reflective) and ceramic (Alumina, SiC) supports on microwave power distributions for oil-in-water (o/w) emulsion samples. Note that, in all cases, the supports (ceramic and/or metallic) are placed at the unexposed face of emulsion slab.

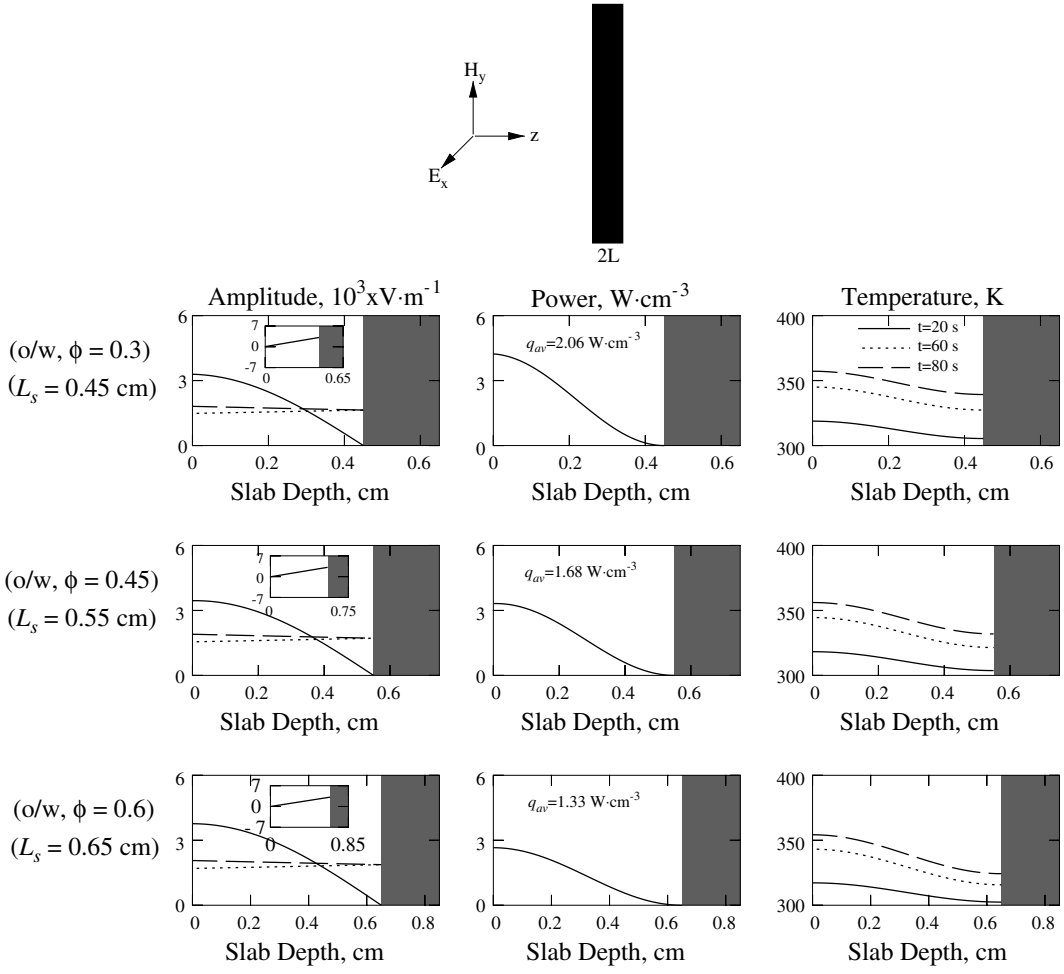

Fig. 4. Amplitudes of electric field ($A_{x,l}, A^t_{x,l}, A^r_{x,l}$), power distributions and temperature profiles for various oil-in-water (o/w) emulsion samples with metallic supports during R_1 mode. The metallic support thickness=0.2 cm. — —, transmitted wave; . . ., reflected wave; —-, stationary wave. The dark shaded regime denotes the metallic support. The inset shows phase difference ($\delta_{x,l}$) vs z.

A preliminary study has been carried out to illustrate the microwave power characteristics for various o/w samples placed on ceramic and/or metallic supports via average power distribution vs emulsion thickness. The average power obtained from Eq. (17) is plotted as a function of emulsion thickness as seen in Fig. 2. The maxima in average power, also termed as 'resonances', are observed for specific emulsion thicknesses and the two consecutive resonances are termed as R_1 and R_2 modes. The significant resonances R_1 and R_2 are due to constructive interferences between transmitted and reflected waves. The amplitudes of the transmitted and reflected waves are generally larger for smaller sample dimensions corresponding to R_1 mode. Hence, the average power at R_1 mode is generally greater than that at R_2 mode irrespective of oil fractions (ϕ) in o/w emulsions. Based on these preliminary studies, specific emulsion thicknesses (L_s) are estimated corresponding to resonances (R_1 and R_2 modes) for enhanced processing of o/w emulsion samples.

Fig. 2a–e illustrate the average power distribution vs emulsion thickness for various o/w emulsion samples placed on metallic support, ceramic supports and composite supports. It is interesting to observe that o/w sample with $\phi = 0.3$ corresponds to greater average power and power absorption decreases with increase in ϕ during both R_1 and R_2 modes for emulsions with metallic support as seen in Fig. 2a. It may also be noted that, emulsion thicknesses corresponding to R_1 and R_2 modes are found to increase with increase in oil fractions (ϕ). In addition, it is observed that composite supports correspond to smaller emulsion thicknesses than that with metallic or individual ceramic supports at R_1 or R_2 mode. It is also observed that average power is quite smaller with larger sample thickness for emulsions with ceramic supports than that for emulsion with metallic support, especially during R_1 mode, for all cases. Note that, power absorption is enhanced significantly with ceramic–metallic composite supports (Alumina-metallic support and SiC-metallic support) compared to the cases with metallic or ceramic supports for both resonance modes (R_1 and R_2). Note that, the average powers (q_{av}) within o/w samples with $\phi = 0.3$ are 2.06, 0.54, 0.23, 3.38 and 2.3 W cm^{-3} for metallic support, Alumina support, SiC support, Alumina-metallic support and SiC-metallic support, respectively, during R_1 mode.

The suitable choice of supports (single or composite) depends on factors such as rate of thermal processing, compositions of emulsions, processing thickness (L_s) and thermal runaway. The interesting features as seen in average power vs emulsion thickness diagram (Fig. 2a–e) provide a suitable guideline in determining the efficient heating strategy for o/w samples with metallic and/or ceramic supports due to microwaves. The detailed analysis of microwave power characteristics and electric field distributions at various resonance modes would be useful to understand the critical role of the specific ceramic and/or metallic supports on optimal thermal processing of emulsions.

Fig. 3 illustrates the spatial distributions of amplitudes of the electric fields, power and temperature for o/w emulsion sample

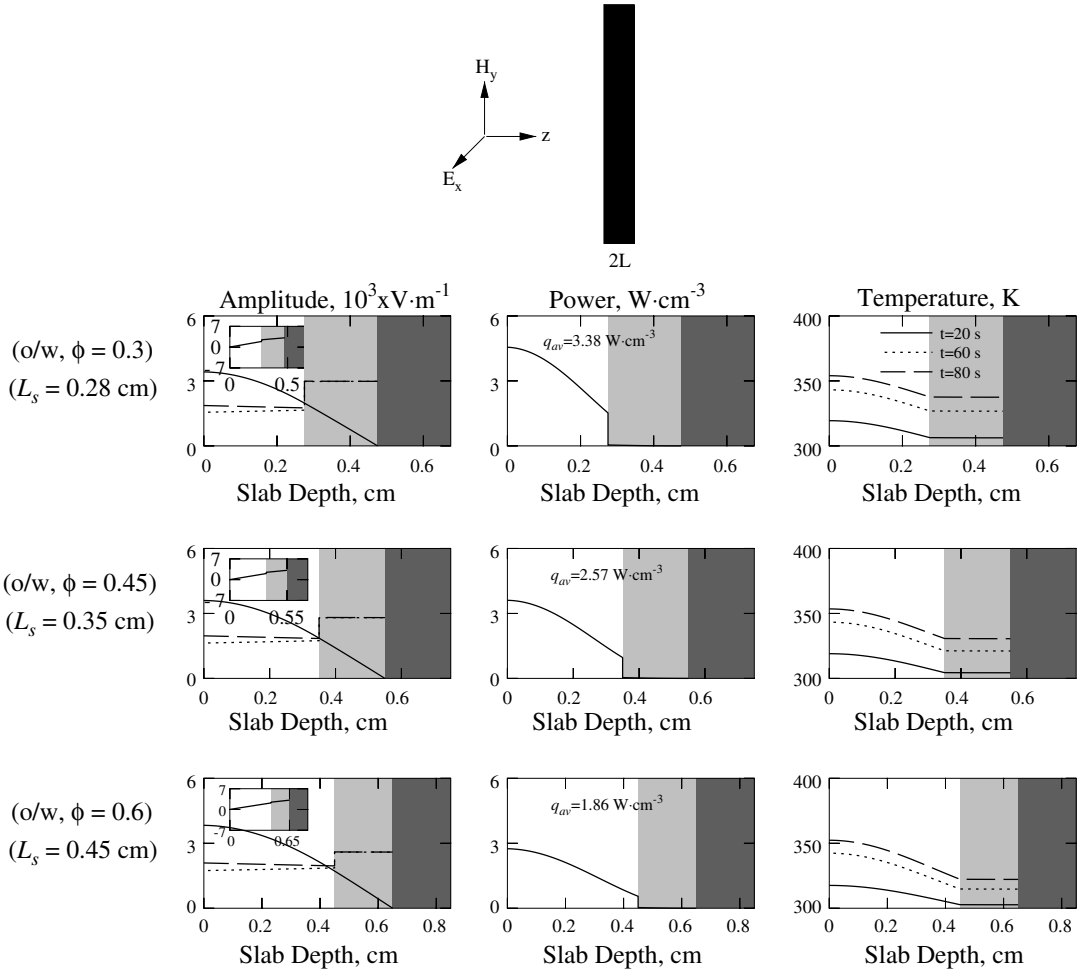

Fig. 5. Amplitudes of electric field ($A_{x,l}, A^t_{x,l}, A^r_{x,l}$), power distributions and temperature profiles for various oil-in-water (o/w) emulsion samples with Alumina-metallic composite supports during R_1 mode. The composite support thickness=0.4 cm. — —, transmitted wave; . . ., reflected wave; —-, stationary wave. The light and dark shaded regimes denote ceramic and metallic support, respectively. The inset shows phase difference ($\delta_{x,l}$) vs z.

with $\phi = 0.3$ for metallic support and ceramic supports (Alumina and SiC) during R_1 mode. Note that, the emulsion thicknesses (L_s) corresponding to R_1 mode are 0.45, 0.88 and 0.78 cm for sample with metallic support, Alumina support and SiC support, respectively. The insets show the difference in phase angles vs distance within the emulsion slabs. The difference in phase angles ($\delta_{x,l}$) illustrates the strength of the stationary wave and zero phase difference signifies the constructive interference, which is also termed as resonance, whereas $\pm\pi$ phase difference signifies the destructive interference. It is observed that, the amplitude of the transmitted wave is larger than that of the reflected wave within the emulsion slab. In addition, the amplitude of the transmitted wave is a decreasing function of distance whereas the amplitude of the reflected wave is an increasing function of distance within the emulsion sample for all the support cases. It is interesting to note that, stationary electric field becomes zero at the unexposed face of sample attached with metallic support due to destructive interference ($\delta_{x,l} = \pi$, as seen in the inset) between transmitted and reflected waves of identical magnitudes. The stationary electric field forms a maxima ($\delta_{x,l} = 0$) at the exposed face of the sample for metallic support. Due to complete conversion of transmitted wave into reflected wave at the unexposed face of the emulsion, significant amount of reflection would cause quite strong interference of waves resulting in greater stationary waves within the emulsion sample in presence of metallic support. Hence, greater power absorption occurs throughout the sample except at the regime near unexposed face. The power distribution follows the same trend as the stationary electric field and the emulsion sample with metallic support corresponds to greater average power ($q_{av} = 2.06\ \mathrm{W\ cm^{-3}}$).

It is interesting to observe that, similar to metallic support, only one spatial resonance or maxima in spatial power occurs at the exposed face of the emulsion sample with SiC support whereas two maxima in spatial power occur at both the surfaces of the sample with Alumina support. The waves do penetrate through and reflect out of the ceramic supports and thus the interference of waves within the sample is coupled with the propagation of waves within ceramic supports. Hence, the stationary wave is not very strong within the emulsion slab which is in contrast with the case of metallic support. It may be noted that, due to low dielectric loss of Alumina ($\kappa'' = 0.1566$) the microwave power absorption is quite small within Alumina support whereas a significant power absorption would occur within SiC support due to very high dielectric loss of SiC ($\kappa'' = 27.99$). Overall, the power distribution follows similar

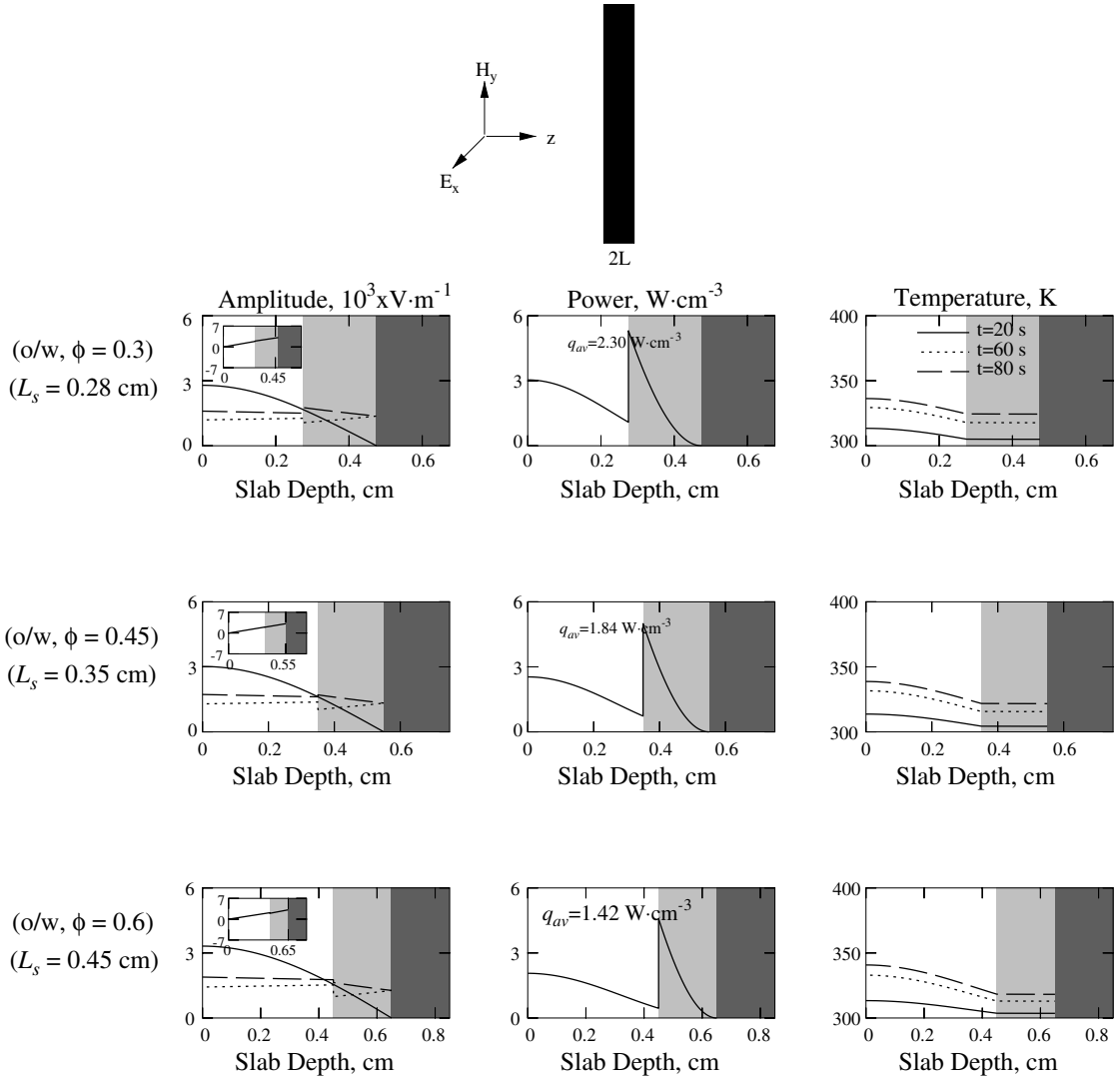

Fig. 6. Amplitudes of electric field ($A_{x,l}, A^t_{x,l}, A^r_{x,l}$), power distributions and temperature profiles for various oil-in-water (o/w) emulsion samples with SiC-metallic composite supports during R_1 mode. The composite support thickness=0.4 cm. — —, transmitted wave; . . ., reflected wave; —·—, stationary wave. The light and dark shaded regimes denote ceramic and metallic support, respectively. The inset shows phase difference ($\delta_{x,l}$) vs z.

trend to the electric field distribution for sample with metallic/ceramic supports. Due to smaller intensity of stationary wave within the sample, power absorption is smaller and the average power within sample is 0.54 W cm^{-3} for Alumina support and 0.23 W cm^{-3} for SiC support. In contrast, average power absorption within sample with metallic support is quite high as mentioned earlier.

The spatial temperature distributions are illustrated for $t = 20$, 60 and 80 s as seen in Fig. 3. It is observed that, during 80 s, the temperature varies within 339.3–357.2 K for sample with metallic support whereas that varies within 307.5–315.6 K and 306.3–309.7 K for sample with Alumina support and SiC support, respectively. Note that, the greater temperature distributions for sample with metallic support are due to greater power depositions which contrasts the cases with ceramic supports. It is also interesting to note that, although the power absorption within the sample regime attached with the metallic support is insignificant, the spatial temperature is significantly high within the regime due to high thermal conductivity of o/w emulsion samples ($\phi = 0.3$). Similar to metallic support case, the spatial temperature is higher at the exposed face than that at the unexposed face for sample with Alumina support whereas it is quite uniform for sample with SiC support due to lower power depositions throughout the sample. Hence, SiC support may be useful to avoid local thermal runaway within o/w emulsion samples.

Fig. 4 illustrates the spatial distributions of amplitudes of the electric fields, power and temperature for o/w emulsion samples with $\phi = 0.3$, 0.45 and 0.6 for metallic support during R_1 mode. The spatial distribution characteristics for o/w emulsion samples with $\phi = 0.3$ have been discussed earlier (Fig. 3). As the spatial distributions are strong functions of ϕ, results have also been reported for various ϕ values in Fig. 4. Note that, the emulsion thicknesses (L_s) corresponding to R_1 mode are 0.45, 0.55 and 0.65 cm for sample with $\phi = 0.3$, 0.45 and 0.6, respectively. Similar to Fig. 3, zero stationary electric field occurs at the unexposed face of samples attached with metallic supports for all cases. It is interesting to observe that, amplitude of the stationary wave increases with increase in ϕ at a specific sample depth. Although the amplitude of the stationary wave is larger within o/w sample with $\phi = 0.6$, the spatial absorption of power within the sample is smaller due to small dielectric loss (κ'') of o/w emulsion sample with $\phi = 0.6$. Note that, average powers (q_{av}) are 2.06, 1.68 and 1.33 W cm^{-3} for sample with $\phi = 0.3$, 0.45 and 0.6, respectively. It may be noted that, only one maxima in spatial power occurs at the exposed face of the sample for all cases. The spatial temperature distributions are illustrated for $t = 20$, 60 and 80 s as seen in Fig. 4. The temper-

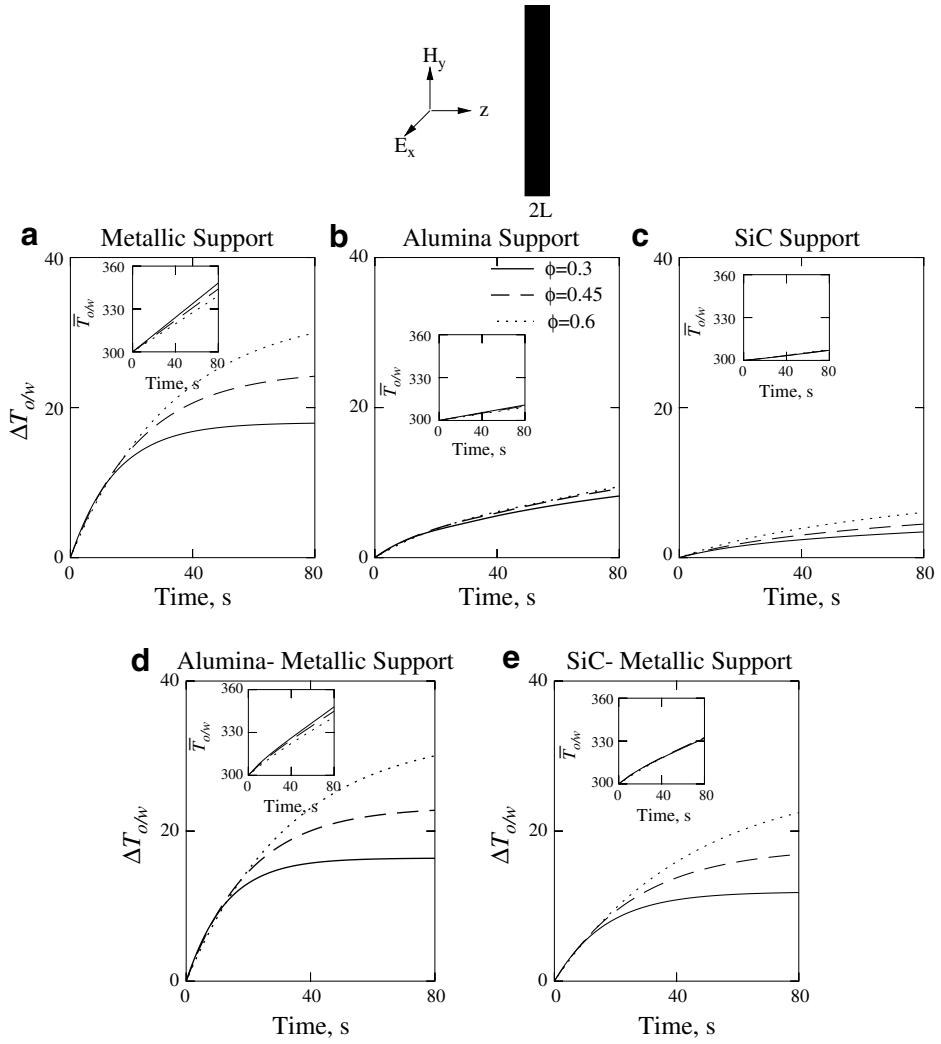

Fig. 7. The temperature difference, $\Delta T_{o/w}$ (K) vs time (s) for various oil-in-water (o/w) emulsion samples with (a) Metallic support, (b) Alumina support, (c) SiC support, (d) Alumina-metallic support and (e) SiC-metallic support, during R_1 mode. The inset shows average temperature, $\overline{T}_{o/w}$ (K) vs time (s).

ature distributions qualitatively follow the power distributions. It is observed that, during 80 s, the temperature varies within 339.3–357.2 K, 331.9–356.1 K and 324.3–354.2 K for o/w emulsions with $\phi = 0.3$, 0.45 and 0.6, respectively. It is interesting to note that, sample with $\phi = 0.6$, which corresponds to the smallest average power, exhibits largest temperature difference within the sample due to smaller effective thermal conductivity. Therefore, the sample with higher oil fraction ($\phi = 0.6$) corresponds to more non-uniform spatial temperature distribution during longer interval of heating time and that may lead to local thermal runaway at the exposed face of the sample.

Although power absorption within emulsion sample is enhanced in the presence of metallic support than that with individual ceramic support, spatial temperature distributions may not meet desired level of uniformity at longer duration of heating, especially for sample with higher oil fractions ($\phi = 0.6$). The role of ceramic–metallic composite support to process emulsion samples will be illustrated next. The specific role of ceramic–metallic composite support will be examined based on various issues. The situation of zero power absorption at the unexposed face of sample attached with metallic support (see Fig. 4) can be avoided. In addition, specific composite support may be useful to reduce local thermal runaway situation resulting in uniform temperature throughout the sample slab.

Fig. 5 illustrates the spatial distributions of amplitudes of the electric fields, power and temperature for o/w emulsion samples with $\phi = 0.3$, 0.45 and 0.6 for Alumina-metallic composite support during R_1 mode. Similar to metallic support cases, the amplitude of the transmitted wave is a decreasing function of distance whereas the amplitude of the reflected wave is an increasing function of distance within the emulsion slab for all cases. It is interesting to observe that there is a significant jump in amplitude of the transmitted and reflected waves within the Alumina support. It may also be noted that, within the support the amplitudes of transmitted and reflected waves are almost equal. Power distributions are seen to qualitatively follow the stationary wave distributions within samples. It may also be noted that, although magnitude of the stationary wave is quite high, spatial power absorption is very less within Alumina support due to smaller dielectric loss of Alumina ($\kappa'' = 0.1566$). Similar to metallic support cases, only one maxima in spatial power occurs at the exposed face of the sample for all cases. Unlike the cases with metallic support (Fig. 4), the unexposed face of the sample attached with Alumina-metallic composite support attains non-zero power absorption. It is also interesting to observe that, average power absorption with Alumina-metallic composite support is greater than that for sample with metallic support for specific oil fractions. Note that, average powers (q_{av}) are 3.38, 2.57 and 1.86 W cm^{-3} for sample with $\phi = 0.3$, 0.45 and 0.6, respectively. It may also be noted that, the emulsion thicknesses (L_s) corresponding to R_1 mode are 0.28, 0.35 and 0.45 cm for sample with $\phi = 0.3$, 0.45 and 0.6, respectively. As the average powers are larger and the emulsion

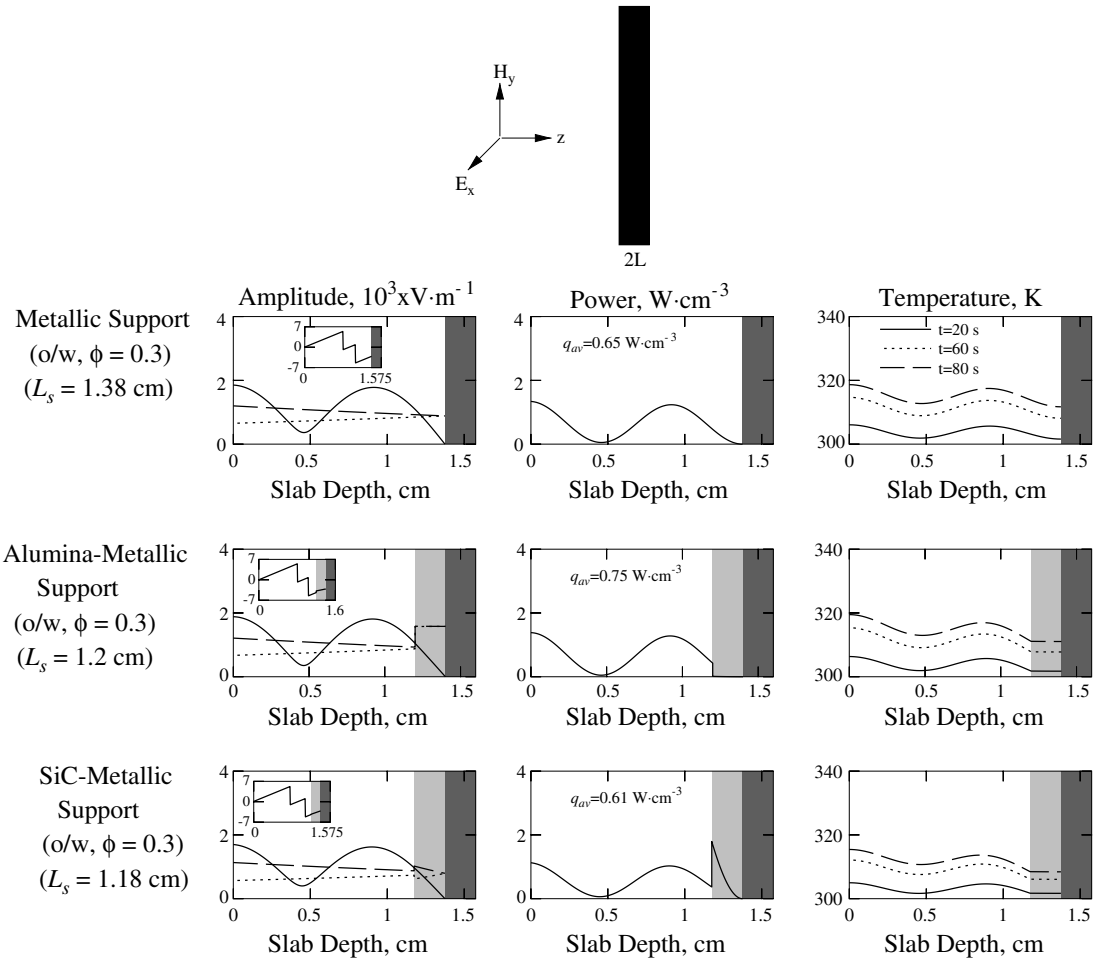

Fig. 8. Amplitudes of electric field ($A_{x,l}, A^t_{x,l}, A^r_{x,l}$), power distributions and temperature profiles for 30% oil-in-water (o/w) emulsion samples with metallic support, Alumina-metallic support and SiC-metallic support, during R_2 mode. The metallic support thickness=0.2 cm and the composite support thickness = 0.4 cm. — —, transmitted wave; . . ., reflected wave; —·—, stationary wave. The light and dark shaded regimes denote ceramic and metallic support, respectively. The inset shows phase difference ($\delta_{x,l}$) vs z.

thicknesses are smaller for Alumina-metallic composite support than that for metallic support, we have also calculated the effective power absorption (numerical values are not shown) in the sample for each case. It is observed that, for the sample with small oil fraction (ϕ), Alumina-metallic composite support corresponds to slightly greater power absorption than that for metallic support whereas for the sample with large oil fraction (ϕ), metallic support corresponds to greater power absorption than that for Alumina-metallic support. The spatial temperature distributions are illustrated for $t = 20$, 60 and 80 s as seen in Fig. 5. During 80 s, the temperature varies within 337.6–354 K, 330.7–353.5 K and 322.3–352.3 K for o/w emulsions with $\phi = 0.3$, 0.45 and 0.6, respectively. Similar to metallic support cases, it is observed that sample with higher oil fraction ($\phi = 0.6$) corresponds to greater temperature difference during longer interval of heating time and that may lead to local thermal runaway situation.

Fig. 6 illustrates the spatial distributions of amplitudes of the electric fields, power and temperature for various o/w emulsion samples with SiC-metallic composite support during R_1 mode. Note that, spatial distributions of traveling waves (transmitted and reflected waves) within the sample are qualitatively similar to Alumina-metallic composite support cases. It is interesting to observe that there is a less significant jump in amplitude of both transmitted and reflected waves within the SiC support and unlike Alumina-metallic composite support cases, reflected wave attains smaller amplitude than that of transmitted wave within the SiC support. Similar to Alumina-metallic composite support cases, power distributions qualitatively follow the stationary wave distributions within samples only. It is interesting to observe that, spatial power absorption shows a high peak at the face of SiC support attached with sample and thereafter spatial power absorption shows a monotonic decrease across SiC support leading to zero value at the SiC-metallic interface. This phenomenon is primarily due to higher dielectric loss of SiC ($\kappa'' = 27.99$). Similar to previous cases, only one maxima in spatial power occurs at the exposed face of the sample and non-zero power absorption occurs at the unexposed face of sample corresponding to SiC-metallic composite support. It is interesting to observe that, average power absorption is lesser with SiC-metallic composite support than that with Alumina-metallic composite support whereas the emulsion thicknesses (L_s) corresponding to R_1 mode are identical for corresponding ϕ values. Note that, average powers (q_{av}) are 2.3, 1.84 and 1.42 W cm^{-3} for sample with $\phi = 0.3$, 0.45 and 0.6, respectively. Based on effective power absorption within the sample for each case, it is observed that SiC-metallic composite support corresponds to smaller power absorption compared to the cases with metallic or Alumina-metallic support for the sample with all ranges of oil fractions (ϕ). Similar to previous cases, the spatial temperature distributions are illustrated for $t = 20$, 60 and 80 s as seen in Fig. 6. During 80 s, the temperature varies within 324.5–336.3 K, 321.8–338.7 K and 318.3–340.8 K for o/w emulsions with $\phi = 0.3$, 0.45 and 0.6, respectively. Unlike metallic support and Alumina-metallic composite support cases, it is observed that the sample with higher oil fraction ($\phi = 0.6$) corresponds to smaller thermal gradient within the sample during longer interval of heating time and that may result in smaller local thermal runaway situation whereas larger local thermal runaway was observed for samples attached with metallic and Alumina-metallic composite supports.

Fig. 7a–e illustrate the temperature difference ($\Delta T_{o/w}$) vs time distributions for various o/w emulsion samples with metallic, ceramic and composite supports during R_1 mode. Note that, temperature difference ($\Delta T_{o/w}$) is defined as the difference between the maximum and minimum temperatures within the emulsion sample and it denotes the degree of thermal runaway. It is interesting to observe that, thermal runaway ($\Delta T_{o/w}$) increases with increase in ϕ values irrespective of the type of support (Fig. 7a–e). It is also observed that, thermal runaway is larger for samples with metallic and ceramic–metallic composite supports whereas thermal runaway is smaller for samples with ceramic (Alumina or SiC) supports. Note that, during 80 s, $\Delta T_{o/w}$ reaches around 30 K when samples ($\phi = 0.6$) are attached with metallic and Alumina-metallic composite supports whereas $\Delta T_{o/w}$ reaches around 22.5 K for samples ($\phi = 0.6$) with SiC-metallic composite supports and $\Delta T_{o/w}$ reaches around 6–9.5 K for samples ($\phi = 0.6$) with ceramic support. The inset illustrates the average temperature ($\overline{T}_{o/w}$) vs time distributions for all the cases. Note that, the slope of the average temperature vs time denotes the heating rate which is directly proportional to the microwave power absorption as the heat loss to the ambiance is neglected (insulated condition). It is interesting to observe that, average temperature ($\overline{T}_{o/w}$) decreases with increase in ϕ values for samples with metallic and Alumina-metallic composite supports and in contrast average temperature for other strategies such as samples with Alumina support, SiC support or SiC-metallic composite support is almost independent of oil contents. It is also observed that, samples with metallic and Alumina-metallic composite supports correspond to greater heating rates whereas heating rates with individual ceramic supports (Alumina or SiC) are quite small for all ranges of oil fractions (ϕ). Note that, for cases with metallic and Alumina-metallic composite supports, average temperature ($\overline{T}_{o/w}$) reaches around 348 K and 340 K during 80 s for samples with $\phi = 0.3$ and 0.6, respectively. On the

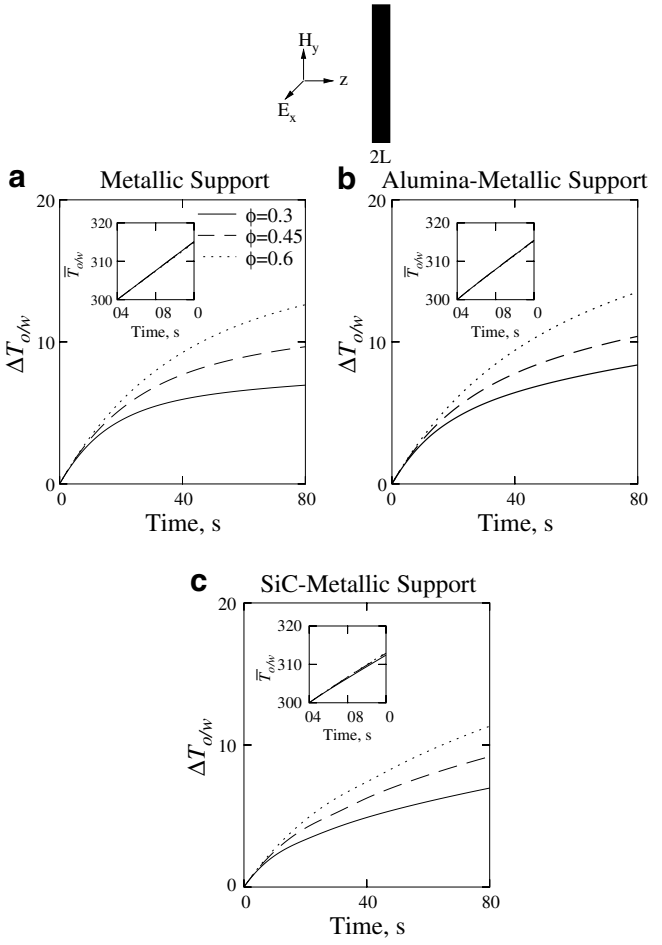

Fig. 9. The temperature difference, $\Delta T_{o/w}$ (K) vs time (s) for various oil-in-water (o/w) emulsion samples with (a) Metallic support, (b) Alumina-metallic support and (c) SiC-metallic support, during R_2 mode. The inset shows average temperature, $\overline{T}_{o/w}$ (K) vs time (s).

other hand, average temperature reaches around 307–310 K during 80 s when samples (for all ϕ values) are processed with ceramic support. It may be inferred that, o/w emulsion samples with SiC-metallic composite supports correspond to reasonably larger heating rates with lesser thermal runaway. An efficient heating strategy for the emulsion-support assembly is characterized by higher rate of thermal processing with smaller thermal runaway. Based on the overall scenarios, SiC-metallic composite support may be chosen as the optimal heating strategy for o/w emulsion samples with higher oil contents ($\phi \geqslant 0.45$) and for samples with smaller oil contents ($\phi = 0.3$), both metallic and Alumina-metallic composite supports are suitable alternatives.

Figs. 3–6 illustrate the spatial distributions of amplitudes of the electric fields, power and temperature for o/w emulsion samples for metallic and/or ceramic supports (Alumina and SiC) during R_1 mode. It may be noted that, the emulsion thicknesses (L_s) corresponding to R_1 mode are quite smaller, especially for sample with metallic, Alumina-metallic and SiC-metallic supports. Hence we have also carried out analysis on spatial distribution for o/w emulsion samples with metallic and/or ceramic supports during R_2 mode which corresponds to larger sample thicknesses. In addition, processing of samples during R_2 mode may be advantageous to achieve less local thermal runaway situation i.e. more uniform heating throughout the sample despite smaller heating rate as discussed next. The detailed spatial distribution for samples with metallic support and composite supports during R_2 mode may be important to analyze further the efficient or optimal thermal processing of o/w emulsion samples. The spatial distributions for individual ceramic support can be similarly deduced and are not shown in this article.

Fig. 8 illustrates the spatial distributions of amplitude, power and temperature for o/w emulsion sample with $\phi = 0.3$ for metallic support, Alumina-metallic support and SiC-metallic support during R_2 mode. Unlike the cases during R_1 mode where only one maxima in spatial power occurs, two maxima in spatial power are observed for all the support assemblies. Similar to previous cases, composite supports correspond to non-zero power absorption at the unexposed face of samples. It is interesting to observe that, average power absorption is enhanced with Alumina-metallic support whereas it is reduced with SiC-metallic support compared to the case with metallic support. Note that, average powers (q_{av}) are 0.65, 0.75 and 0.61 W cm^{-3} for sample with metallic support, Alumina-metallic support and SiC-metallic support, respectively, during R_2 mode. Note that, the emulsion thicknesses (L_s) corresponding to R_2 mode are 1.38, 1.2 and 1.18 cm for sample with metallic support, Alumina-metallic support and SiC-metallic support, respectively. As the average power is larger and the emulsion thickness is smaller for Alumina-metallic support than that for

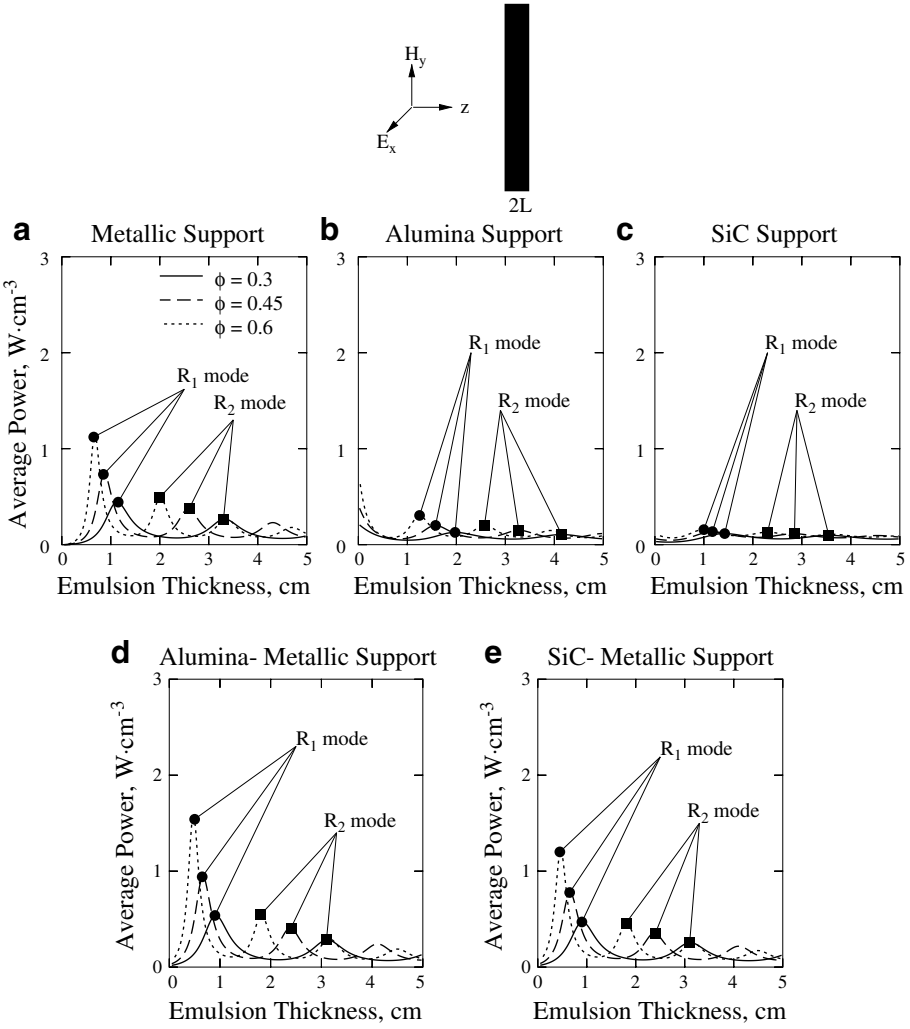

Fig. 10. Average power (W cm^{-3}) vs emulsion thickness (cm) for various water-in-oil (w/o) emulsion samples with (a) Metallic support, (b) Alumina support, (c) SiC support, (d) Alumina-metallic support and (e) SiC-metallic support. The symbol, ●, denotes R_1 mode and the symbol, ■, denotes R_2 mode of resonances.

metallic support, based on effective power absorption it is observed that, both correspond to almost identical power absorption. Similar to previous cases, the spatial temperature distributions are illustrated for $t = 20$, 60 and 80 s as seen in Fig. 8. During 80 s, the temperature varies within 311.7–318.7 K, 311.1–319.5 K and 308.5–315.4 K for o/w emulsions with metallic support, Alumina-metallic support and SiC-metallic support, respectively. It is interesting to observe that, heating is quite uniform throughout the sample for all the support assemblies and this avoids local thermal runaway situation even at longer duration of heating time. This is in contrast for cases during R_1 mode which corresponds to significant thermal runaway situation especially for samples with metallic and Alumina-metallic supports.

Fig. 9a–c illustrate the temperature difference ($\Delta T_{o/w}$) vs time distributions for various o/w emulsion samples with metallic and composite supports during R_2 mode. Similar to the cases during R_1 mode, it is observed that thermal runaway ($\Delta T_{o/w}$) increases with increase in ϕ values irrespective of the type of support (Fig. 9a–c). In addition, temperature difference ($\Delta T_{o/w}$) for cases with metallic and Alumina-metallic supports is slightly larger than that for cases with SiC-metallic support. It is interesting to observe that, unlike the cases during R_1 mode, thermal runaway is quite smaller for all cases irrespective of supports. Note that, during 80 s, $\Delta T_{o/w}$ reaches around 13 K when samples ($\phi = 0.6$) are attached with metallic and Alumina-metallic supports whereas $\Delta T_{o/w}$ reaches around 11 K when samples ($\phi = 0.6$) are attached with SiC-metallic support. The inset illustrates the average temperature ($\overline{T}_{o/w}$) vs time distributions for all the cases. It is interesting to observe that, unlike the cases during R_1 mode, average temperature ($\overline{T}_{o/w}$) is almost independent of ϕ values for all the support assemblies. It is also observed that, samples with metallic and Alumina-metallic composite supports correspond to slightly greater heating rates than that with SiC-metallic support. Note that, for cases with both metallic and Alumina-metallic composite supports, average temperature ($\overline{T}_{o/w}$) reaches around 315 K whereas that reaches around 313 K when samples are processed with SiC-metallic support during 80 s. Based on the scenarios corresponding to R_2 mode, both metallic and Alumina-metallic supports may be suitable as the optimal heating strategy for o/w emulsion samples for all ranges of oil contents (ϕ) as both the strategies correspond to reasonably large heating rates with smaller thermal runaway.

3.2. Microwave power and temperature distributions for water-in-oil (w/o) emulsions

Fig. 10a–e illustrate the average power distribution vs emulsion thickness for various w/o emulsion samples placed on metallic and/or ceramic supports. It is interesting to observe that, unlike o/w cases (Fig. 2a–e), w/o sample with $\phi = 0.3$ corresponds to smaller average power and power absorption increases with increase in ϕ during both R_1 and R_2 modes for emulsions with all support assemblies. This is due to the fact that effective dielectric

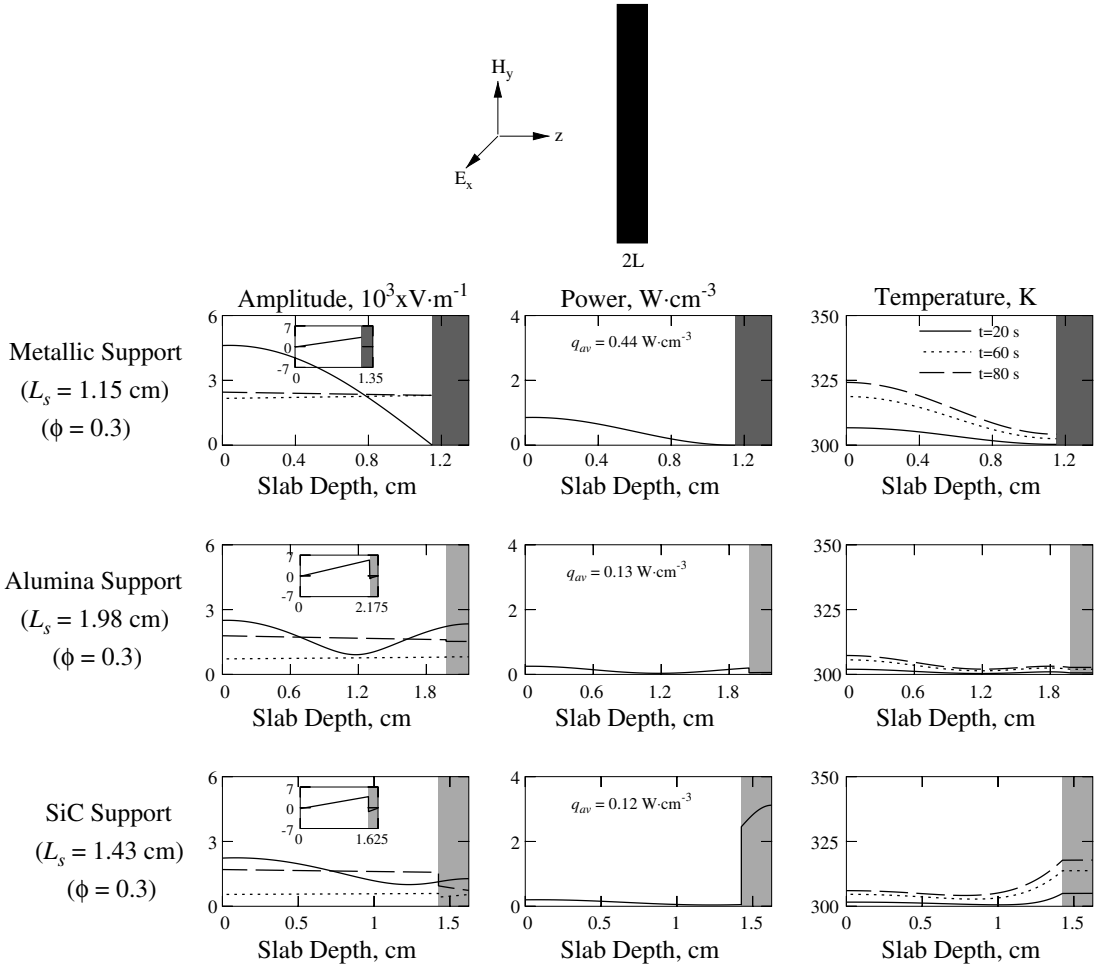

Fig. 11. Amplitudes of electric field ($A_{x,l}, A^t_{x,l}, A^r_{x,l}$), power distributions and temperature profiles for 30% water-in-oil (w/o) emulsion samples with metallic support, Alumina support and SiC support during R_1 mode. The support thickness = 0.2 cm. — —, transmitted wave; . . ., reflected wave; —·—, stationary wave. The light and dark shaded regimes denote ceramic and metallic support, respectively. The inset shows phase difference ($\delta_{x,l}$) vs z.

loss increases with ϕ for w/o samples. It is also observed that, emulsion thicknesses corresponding to R_1 and R_2 modes decrease with increase in water fractions (ϕ). In addition, composite supports correspond to smaller emulsion thicknesses than that with metallic or individual ceramic supports at a specific resonance mode (R_1 or R_2). Similar to o/w cases, metallic support corresponds to greater average power than that with ceramic supports and power absorption is enhanced significantly for samples with composite supports especially with Alumina-metallic support as seen in Fig. 10a–e. Note that, the average powers (q_{av}) within w/o samples with $\phi = 0.3$ and 0.6 are 0.54 and 1.54 W cm^{-3}, respectively for Alumina-metallic support whereas the average powers for samples with $\phi = 0.3$ and 0.6 are 0.12 and 0.16 W cm^{-3}, respectively for SiC support, during R_1 mode.

Fig. 11 illustrates the spatial distributions of amplitude, power and temperature for w/o emulsion sample with $\phi = 0.3$ for metallic support and ceramic supports during R_1 mode. The spatial distributions of amplitudes of the traveling and stationary waves are qualitatively similar to those of o/w cases (Fig. 3). Similar to o/w cases, the stationary electric field forms a maxima at the exposed face of samples with metallic support. The power distribution follows the same trend as the stationary electric field. Similar to metallic support, only one maxima in spatial power occurs at the exposed face of the emulsion sample with SiC support whereas two maxima in spatial power occur at both the surfaces of the sample with Alumina support. It is observed that, average power absorption within sample with metallic support is larger (0.44 W cm^{-3}) due to significant reflection within the metallic support whereas power absorptions within samples with ceramic supports are quite less (0.13 W cm^{-3} for Alumina support and 0.12 W cm^{-3} for SiC support). Note that, the emulsion thicknesses (L_s) corresponding to R_1 mode are 1.15, 1.98 and 1.43 cm for sample with metallic support, Alumina support and SiC support, respectively. Based on effective power absorption, metallic support corresponds to greater power than that with ceramic supports. The spatial temperature distributions are illustrated for $t = 20$, 60 and 80 s as seen in Fig. 11. It is observed that, during 80 s, the temperature varies within 304.2–324.2 K for sample with metallic support whereas that varies within 302–307.3 K and 304.2–317.8 K for sample with Alumina support and SiC support, respectively.

Fig. 12 illustrates the spatial distributions of amplitude, power and temperature for various w/o emulsion samples with metallic support during R_1 mode. The spatial distributions are qualitatively similar to those of o/w cases (Fig. 4). Similar to Fig. 4, zero stationary electric field occurs at the unexposed face of samples attached with metallic supports and one maxima in spatial power occurs at the exposed face of the sample. It is interesting to observe that, unlike o/w cases, the emulsion thickness (L_s) decreases and power absorption increases with increase in ϕ. Note that, the emulsion

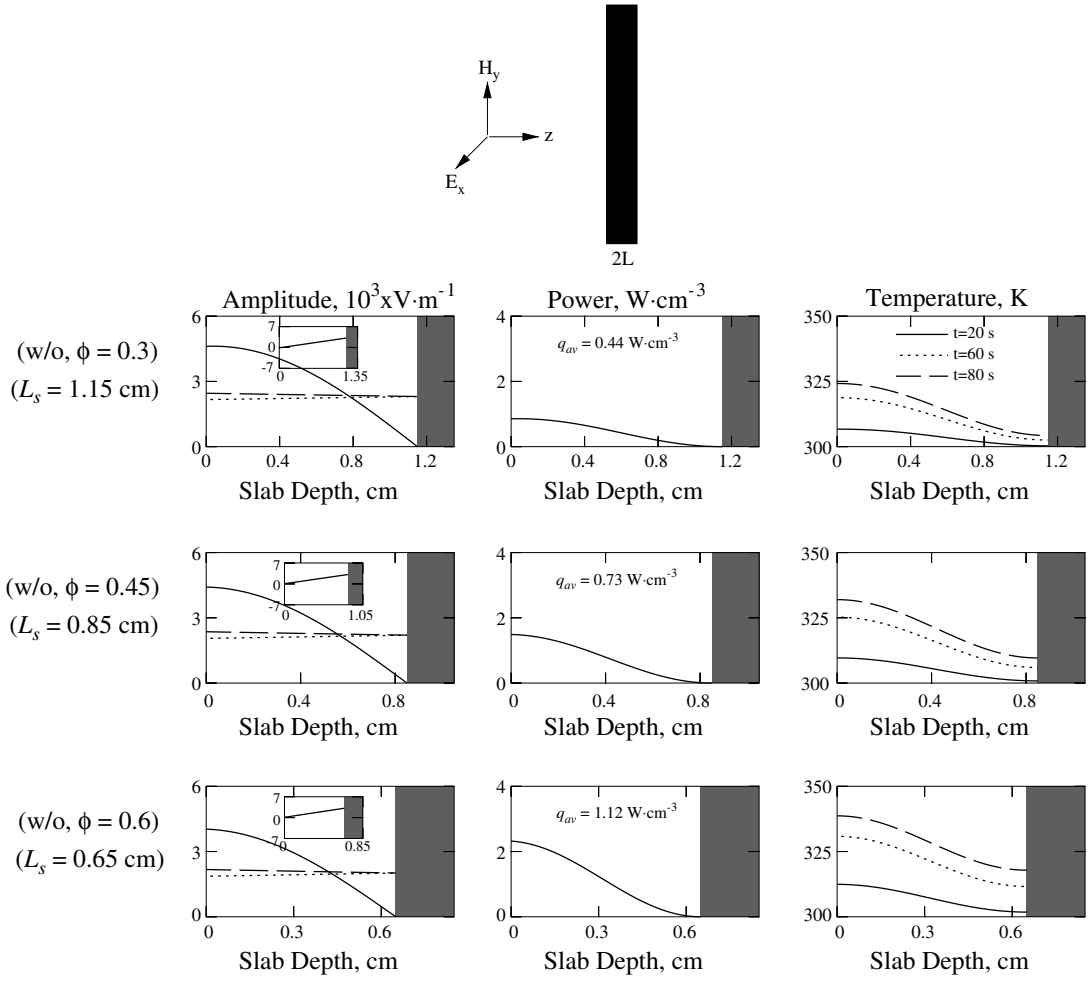

Fig. 12. Amplitudes of electric field ($A_{x,l}, A^t_{x,l}, A^r_{x,l}$), power distributions and temperature profiles for various water-in-oil (w/o) emulsion samples with metallic supports during R_1 mode. The metallic support thickness=0.2 cm. — —, transmitted wave; . . ., reflected wave; —-, stationary wave. The dark shaded regime denotes the metallic support. The inset shows phase difference ($\delta_{x,l}$) vs z.

thicknesses (L_s) corresponding to R_1 mode are 1.15, 0.85 and 0.65 cm for sample with $\phi = 0.3$, 0.45 and 0.6, respectively. In addition, Average powers (q_{av}) are 0.44, 0.73 and 1.12 W cm^{-3} for sample with $\phi = 0.3$, 0.45 and 0.6, respectively. Although the amplitude of the stationary wave is larger within sample with $\phi = 0.3$, the spatial absorption of power within the sample is smaller due to low dielectric loss (κ'') of w/o emulsion sample with $\phi = 0.3$. The spatial temperature distributions are illustrated for $t = 20$, 60 and 80 s as seen in Fig. 12. Note that, the temperature distributions qualitatively follow the power distributions. It is observed that, during 80 s, the temperature varies within 304.2–324.2 K, 309.6–332 K and 317.9–338.7 K for sample with $\phi = 0.3$, 0.45 and 0.6, respectively. Common to all the water fractions is the similar degree of thermal runaway during longer interval of heating time and that may lead to local thermal runaway situation at the exposed face of the sample.

Fig. 13 illustrates the spatial distributions of amplitude, power and temperature for various w/o emulsion samples with Alumina-metallic composite support during R_1 mode. Note that, the variations of amplitudes of the traveling and stationary waves are qualitatively similar to those of o/w cases as seen in Fig. 5. It is interesting to observe that unlike o/w emulsion, there is less significant jump in amplitude of the transmitted and reflected wave within the Alumina support. Note that, the amplitudes of transmitted and reflected waves within the support are almost equal. Similar to o/w cases, the stationary electric field forms a maxima at the exposed face of samples. Note that, power distributions qualitatively follow the stationary wave distributions within samples and hence one maxima in spatial power i.e. resonance occurs at the exposed face of the sample. Similar to o/w emulsion cases (Fig. 5), the unexposed face of the sample attached with Alumina-metallic support attains non-zero power absorption. It is interesting to observe that, average power absorption is enhanced with slightly reduced sample thickness (L_s) for Alumina-metallic composite support compared to the cases with metallic support. Note that, average powers (q_{av}) are 0.54, 0.94 and 1.54 W cm^{-3} for sample with $\phi = 0.3$, 0.45 and 0.6, respectively. In addition, the emulsion thicknesses (L_s) corresponding to R_1 mode are 0.9, 0.65 and 0.5 cm for sample with $\phi = 0.3$, 0.45 and 0.6, respectively. It is observed that for the sample with larger water fraction (ϕ), Alumina-metallic support corresponds to greater effective power absorption (q_{eff}) than that with metallic support whereas for the sample with small water fraction (ϕ), metallic support corresponds to slightly greater effective power absorption than that with Alumina-metallic support. The spatial temperature distributions are illustrated for $t = 20$, 60 and 80 s as seen in Fig. 13. During 80 s, the temperature varies within 304.2–324.3 K, 309.4–331.7 K and 317.2–338.9 K for w/o emulsions with $\phi = 0.3$, 0.45 and 0.6, respectively. Similar to metallic support cases, degree of thermal runaway is significant during longer interval of heating time and that may lead to local thermal runaway situation at the exposed face of the sample.

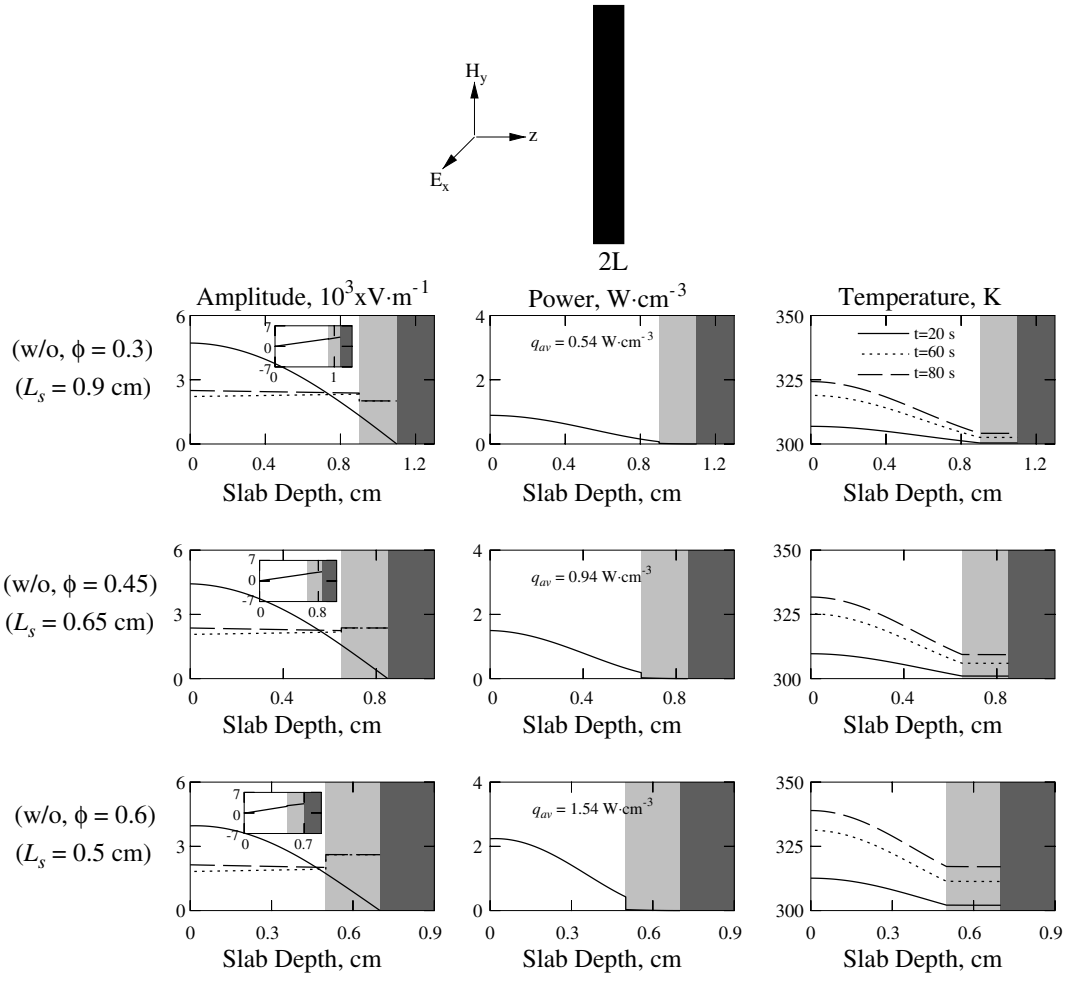

Fig. 13. Amplitudes of electric field ($A_{x,l}, A^t_{x,l}, A^r_{x,l}$), power distributions and temperature profiles for various water-in-oil (w/o) emulsion samples with Alumina-metallic composite supports during R_1 mode. The composite support thickness=0.4 cm. — —, transmitted wave; . . ., reflected wave; —-, stationary wave. The light and dark shaded regimes denote ceramic and metallic support, respectively. The inset shows phase difference ($\delta_{x,l}$) vs z.

We have also carried out the spatial distributions of amplitude, power and temperature for various w/o emulsion samples with SiC-metallic composite support during R_1 mode (Figures not shown). Note that, the variations of amplitudes, powers and temperatures are qualitatively similar to the earlier case of o/w samples as seen in Fig. 6. The spatial temperature varies within 308.6–321.2 K, 312.4–326.8 K and 317.1–330.2 K for w/o emulsions with $\phi = 0.3$, 0.45 and 0.6, respectively, during 80 s. Unlike metallic and Alumina-metallic composite support cases, it is observed that the samples with all ranges of water fraction (ϕ) correspond to lesser thermal gradients within the samples during longer interval of heating time leading to lesser local thermal runaway situation.

Fig. 14a–e illustrate the temperature difference ($\Delta T_{w/o}$) vs time distributions for various w/o emulsion samples with metallic and/or ceramic supports during R_1 mode. It is interesting to observe that, thermal runaway ($\Delta T_{w/o}$) is a strong function of type of supports whereas water fractions have a little influence on thermal runaway. Note that, thermal runaway is larger for samples with metallic and Alumina-metallic composite supports whereas thermal runaway is smaller for samples with Alumina support. In addition, for metallic and Alumina-metallic composite supports, samples with larger water fractions ($\phi = 0.6$) correspond to larger thermal runaway situations than that for samples with smaller water fractions during initial stages of heating ($t \leqslant 60$ s) and $\Delta T_{w/o}$ is reduced significantly during later stages of heating. Consequently, $\Delta T_{w/o}$ values are seen to merge within a short ranges of temperature at a large time ($t = 80$ s) for samples with all water fractions (ϕ). Note that, during 80 s, $\Delta T_{w/o}$ reaches around 20–22 K when samples are attached with metallic and Alumina-metallic composite supports whereas $\Delta T_{w/o}$ is around 12.5–14 K for samples with SiC-metallic support and that reaches around 5–6.5 K for samples with Alumina support.

The inset illustrates the average temperature ($\overline{T}_{w/o}$) vs time distributions for all the cases (Fig. 14). It is interesting to observe that, average temperature ($\overline{T}_{w/o}$) increases with increase in ϕ values for samples with metallic and composite supports and in contrast average temperature is almost independent of water contents for samples with ceramic supports. It is also observed that, samples with metallic and Alumina-metallic composite supports correspond to greater heating rates whereas heating rate with SiC-metallic composite support is slightly less. In addition, the heating rate with individual ceramic supports (Alumina or SiC) are quite small for all ranges of water fractions. Note that, for cases with metallic and Alumina-metallic composite supports, average temperature ($\overline{T}_{w/o}$) reaches around 314.5–316 K and 328–330 K during

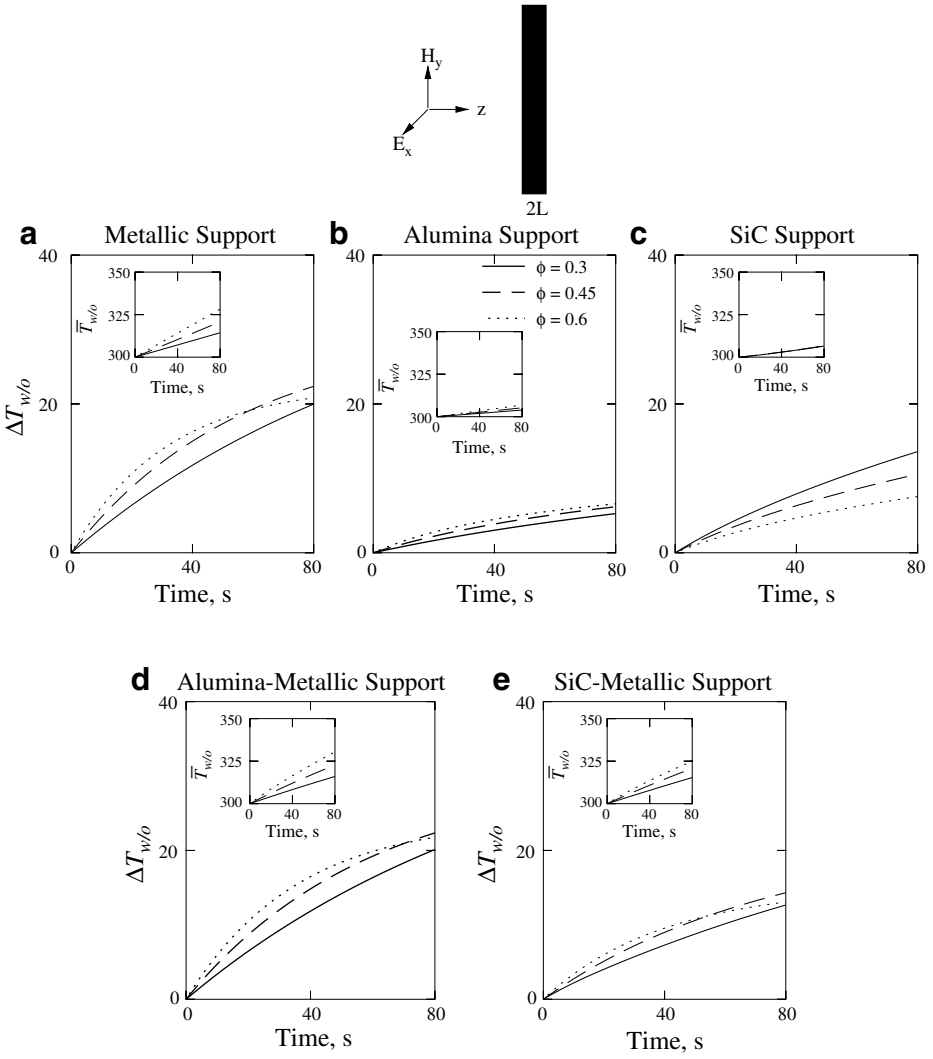

Fig. 14. The temperature difference, $\Delta T_{w/o}$ (K) vs time (s) for various water-in-oil (w/o) emulsion samples with (a) Metallic support. (b) Alumina support. (c) SiC support. (d) Alumina-metallic support and (e) SiC-metallic support, during R_1 mode. The inset shows average temperature, $\overline{T}_{w/o}$ (K) vs time (s).

80 s for samples with $\phi = 0.3$ and 0.6, respectively whereas average temperature reaches around 306 K during 80 s when samples (for all ϕ values) are processed with ceramic supports. It is also observed that, w/o emulsion samples with SiC-metallic composite supports correspond to large heating rates ($\overline{T}_{w/o} = 325$K for sample with $\phi = 0.6$) with controlled thermal runaway. Based on the overall scenarios, SiC-metallic composite support may be chosen as the optimal heating strategy for w/o emulsion samples with all ranges of water fractions (ϕ).

It may be noted from Fig. 10a–e that, the emulsion thicknesses (L_s) corresponding to R_1 mode are quite smaller, especially for sample with higher water fractions ($\phi = 0.6$) for metallic support, Alumina-metallic support and SiC-metallic support. Therefore, we have also carried out analysis on spatial distribution for w/o emulsion samples with metallic and/or ceramic supports during R_2 mode which corresponds to larger sample thicknesses. In addition, processing of samples during R_2 mode may be advantageous to achieve more uniform heating throughout the sample. The detailed spatial distribution for samples with metallic support and composite supports during R_2 mode may be important to analyze further the efficient or optimal thermal processing of w/o emulsion samples.

Fig. 15 illustrates the spatial distributions of amplitude, power and temperature for w/o emulsion sample with $\phi = 0.6$ for metallic support, Alumina-metallic support and SiC-metallic support during R_2 mode. Note that, the variations of amplitudes, powers and temperatures are qualitatively similar to the earlier case of o/w samples as seen in Fig. 8. Unlike the cases during R_1 mode where only one maxima occurs, two maxima in spatial power are observed for all the support assemblies. Similar to previous cases, composite supports correspond to non-zero power absorption at the unexposed face of samples. It is interesting to observe that, average power absorption is enhanced with Alumina-metallic support whereas it is reduced with SiC-metallic support compared to the case with metallic support. Note that, average powers (q_{av}) are 0.49, 0.54 and 0.46 W cm^{-3} for sample with metallic support, Alumina-metallic support and SiC-metallic support, respectively, during R_2 mode. In addition, the emulsion thicknesses (L_s) corresponding to R_2 mode are 2, 1.8 and 1.8 cm for sample with metallic support, Alumina-metallic support and SiC-metallic support, respectively. Based on effective power absorption it is observed that, both metallic and Alumina-metallic supports correspond to almost equal power absorption whereas SiC-metallic support corresponds to slightly less power absorption. The spatial temperature distributions are illustrated for $t = 20$, 60 and 80 s as seen in Fig. 15. During 80 s, the temperature varies within 307.5–317.2 K, 307.4–317.2 K and 307–314.7 K for w/o emulsions with metallic support, Alumina-metallic support and SiC-metallic support, respectively. It is interesting to observe that, heating is almost uniform throughout the sample for all the

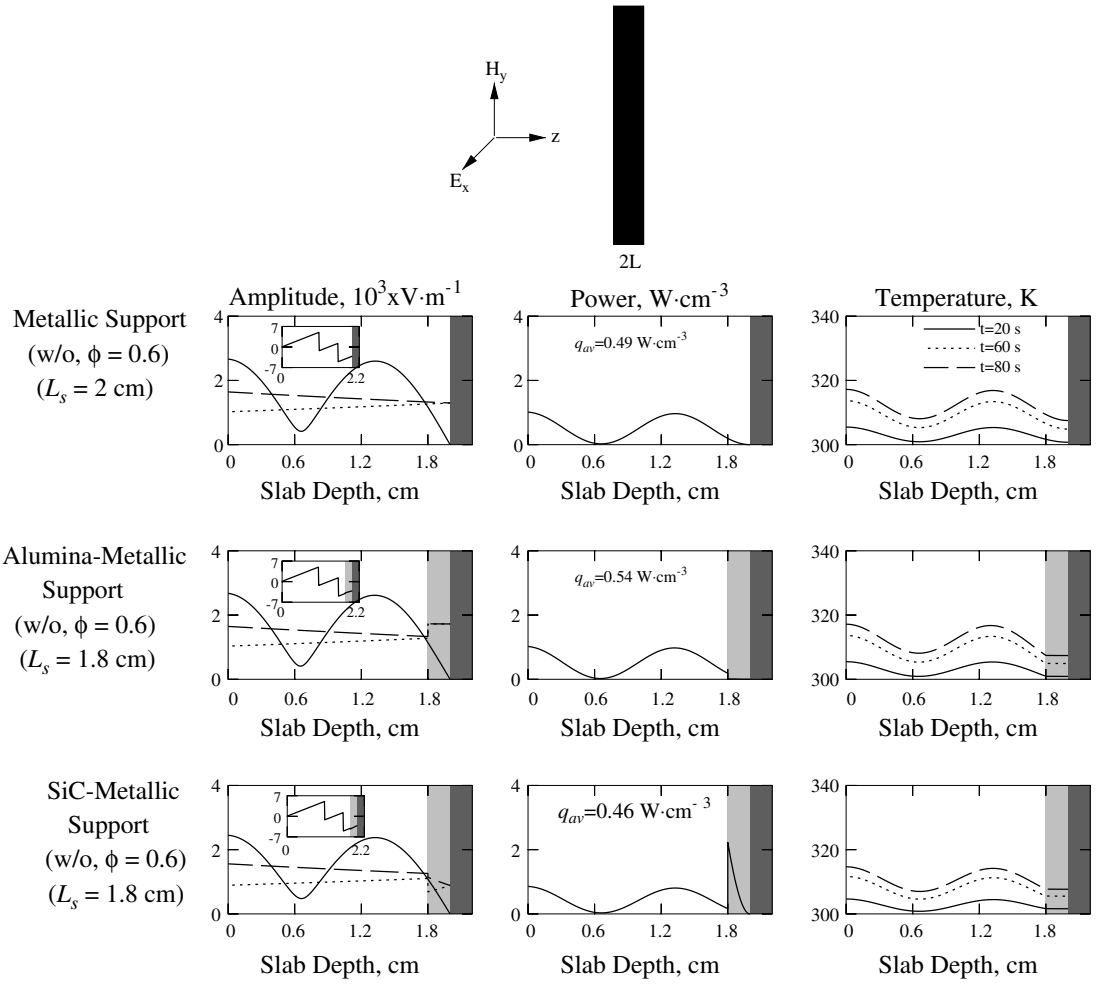

Fig. 15. Amplitudes of electric field ($A_{x,l}, A^t_{x,l}, A^r_{x,l}$), power distributions and temperature profiles for 60% water-in-oil (w/o) emulsion samples with metallic support, Alumina-metallic support and SiC-metallic support, during R_2 mode. The metallic support thickness = 0.2 cm and the composite support thickness = 0.4 cm. — —, transmitted wave; …, reflected wave; —-, stationary wave. The light and dark shaded regimes denote ceramic and metallic support, respectively. The inset shows phase difference ($\delta_{x,l}$) vs z.

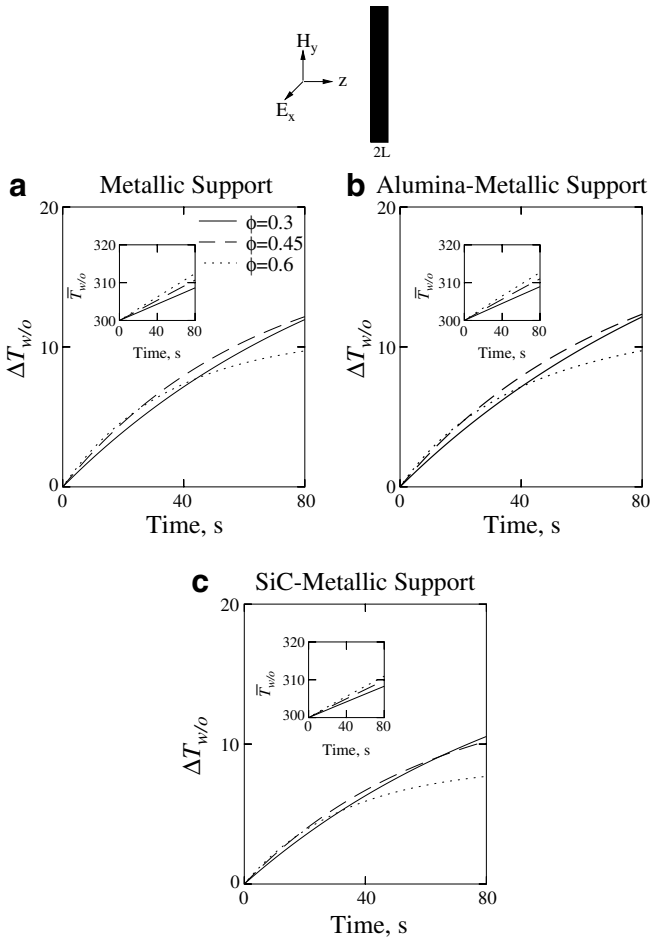

Fig. 16. The temperature difference, $\Delta T_{w/o}$ (K) vs time (s) for various water-in-oil (w/o) emulsion samples with (a) Metallic support. (b) Alumina-metallic support and (c) SiC-metallic support, during R_2 mode. The inset shows average temperature, $\overline{T}_{w/o}$ (K) vs time (s).

support assemblies and this avoids local thermal runaway situation even at longer duration of heating time. This is in contrast for samples processed during R_1 mode which corresponds to significant thermal runaway situation especially with metallic and Alumina-metallic support cases.

Fig. 16a–c illustrate the temperature difference ($\Delta T_{w/o}$) vs time distributions for various w/o emulsion samples with metallic and composite supports during R_2 mode. Unlike the cases during R_1 mode, it is interesting to observe that samples with higher water fractions ($\phi = 0.6$) correspond to smaller thermal runaway situations than that for samples with smaller water fractions during later stages of heating ($t \geqslant 50$ s). Overall, the degree of thermal runaway ($\Delta T_{w/o}$) is less for all ϕ values compared to the cases during R_1 mode for all support-assemblies. Note that, during 80 s, $\Delta T_{w/o}$ reaches around 10–12 K when samples are attached with metallic and Alumina-metallic supports whereas $\Delta T_{w/o}$ reaches around 8–10 K when samples are attached with SiC-metallic support. The inset illustrates the average temperature ($\overline{T}_{w/o}$) vs time distributions for all the cases. It is interesting to observe that, unlike the o/w cases during R_2 mode (Fig. 9a–c), average temperature ($\overline{T}_{w/o}$) increases with increase in ϕ values for all cases. It is also observed that, samples with metallic and Alumina-metallic supports correspond to slightly greater heating rates than that with SiC-metallic support. Note that, for cases with both metallic and Alumina-metallic supports, average temperature ($\overline{T}_{w/o}$) reaches around 309–312.5 K whereas that reaches around 308–311 K when samples are processed with SiC-metallic support during 80 s. Based on the scenarios corresponding to R_2 mode, both metallic and Alumina-metallic supports may be suitable as the optimal heating strategy for w/o emulsion samples for all ranges of water fractions (ϕ).

4. Conclusions

Extensive studies have been carried out to investigate the influence of various ceramic supports, metallic (reflective) supports and ceramic–metallic composite supports on microwave processing of oil–water emulsion samples. The case studies have been carried out for various fractions (ϕ) of dispersed phase corresponding to each type of emulsion. A preliminary analysis has been carried out via average power vs sample thickness diagram to estimate microwave power absorption within emulsion samples for each case. The maxima in average power, also termed as 'resonances', are observed for specific emulsion thicknesses and the two consecutive resonances of significant magnitudes are termed as R_1 and R_2

Table 2
The summary of microwave heating characteristics for oil-in-water (o/w) emulsion samples corresponding to metallic and composite supports

Strategy	Composition	Significant features (R_1 mode)	Significant features (R_2 mode)
Metallic support	Larger oil fraction ($\phi \geqslant 0.45$)	• Heating rate is large ($\overline{T} = 339.3 - 344$ K at 80 s) • Thermal runaway is significant ($\Delta T = 24.2 - 30$ K at 80 s)	• Thermal runaway is smaller ($\Delta T = 9.7 - 12.6$ K at 80 s) • Processing thickness is large ($L_s = 1.65 - 1.95$ cm)
	Smaller oil fraction ($\phi = 0.3$)	• Heating rate is large ($\overline{T} = 348.2$ K at 80 s) • Thermal runaway is smaller ($\Delta T = 17.9$ K at 80 s)	• Thermal runaway is quite small ($\Delta T = 7$ K at 80 s) • Processing thickness is large ($L_s = 1.38$ cm)
Alumina-metallic support	Larger oil fraction ($\phi \geqslant 0.45$)	• Heating rate is large ($\overline{T} = 340.8 - 344.9$ K at 80 s) • Thermal runaway is significant ($\Delta T = 22.8 - 30$ K at 80 s)	• Thermal runaway is smaller ($\Delta T = 10.4 - 13.5$ K at 80 s) • Processing thickness is large ($L_s = 1.45 - 1.75$ cm)
	Smaller oil fraction ($\phi = 0.3$)	• Heating rate is large ($\overline{T} = 347.9$ K at 80 s) • Thermal runaway is smaller ($\Delta T = 16.4$ K at 80 s)	• Thermal runaway is quite small ($\Delta T = 8.4$ K at 80 s) • Processing thickness is large ($L_s = 1.2$ cm)
SiC- Metallic support	Larger oil fraction ($\phi \geqslant 0.45$)	• Heating rate is moderate ($\overline{T} = 332.4$ K at 80 s) • Thermal runaway is smaller ($\Delta T = 16.9 - 22.5$ K at 80 s)	• Thermal runaway is smaller ($\Delta T = 9.2 - 11.3$ K at 80 s) • Processing thickness is large ($L_s = 1.45 - 1.75$ cm)
	Smaller oil fraction ($\phi = 0.3$)	• Heating rate is moderate ($\overline{T} = 332$ K at 80 s) • Thermal runaway is smaller ($\Delta T = 11.8$ K at 80 s)	• Thermal runaway is quite small ($\Delta T = 7$ K at 80 s) • Processing thickness is large ($L_s = 1.18$ cm)
Recommendations		• SiC-metallic support is the optimal heating strategy for o/w emulsions with larger oil fractions ($\phi \geqslant 0.45$) during R_1 mode • Metallic and Alumina-metallic supports are suitable strategies for o/w samples with smaller oil fractions ($\phi = 0.3$) during R_1 mode • Metallic and Alumina-metallic supports are suitable strategies for o/w samples with larger processing thickness corresponding to R_2 mode (for all ϕ values)	

Table 3
The summary of microwave heating characteristics for water-in-oil (w/o) emulsion samples corresponding to metallic and composite supports

Strategy	Composition	Significant features (R_1 mode)	Significant features (R_2 mode)
Metallic support	Larger water fraction ($\phi \geqslant 0.45$)	• Heating rate is large ($\overline{T} = 320.7 - 328.2$ K at 80 s) • Thermal runaway is significant ($\Delta T = 20.8 - 22.4$ K at 80 s)	• Thermal runaway is smaller ($\Delta T = 9.7 - 12.2$ K at 80 s) • Processing thickness is large ($L_s = 2 - 2.7$ cm)
	Smaller water fraction ($\phi = 0.3$)	• Processing thickness is large ($L_s = 1.15$ cm) • Thermal runaway is significant ($\Delta T = 20$ K at 80 s)	• Processing thickness is very large ($L_s = 3.3$ cm) • Thermal runaway is small ($\Delta T = 12$ K at 80 s)
Alumina-metallic support	Larger water fraction ($\phi \geqslant 0.45$)	• Heating rate is large ($\overline{T} = 322.8 - 330.5$ K at 80 s) • Thermal runaway is significant ($\Delta T = 21.8 - 22.4$ K at 80 s)	• Thermal runaway is smaller ($\Delta T = 9.7 - 12.3$ K at 80 s) • Processing thickness is large ($L_s = 1.8 - 2.3$ cm)
	Smaller water fraction ($\phi = 0.3$)	• Processing thickness is large ($L_s = 0.9$ cm) • Thermal runaway is significant ($\Delta T = 20.1$ K at 80 s)	• Processing thickness is very large ($L_s = 3.1$ cm) • Thermal runaway is small ($\Delta T = 12.2$ K at 80 s)
SiC-metallic support	Larger water fraction ($\phi \geqslant 0.45$)	• Heating rate is moderate ($\overline{T} = 320.7 - 325$ K at 80 s) • Thermal runaway is smaller ($\Delta T = 13.1 - 14.3$ K at 80 s)	• Thermal runaway is smaller ($\Delta T = 7.7 - 10.2$ K at 80 s) • Processing thickness is large ($L_s = 1.8 - 2.3$ cm)
	Smaller water fraction ($\phi = 0.3$)	• Processing thickness is large ($L_s = 0.9$ cm) • Thermal runaway is small ($\Delta T = 12.7$ K at 80 s)	• Processing thickness is very large ($L_s = 3.1$ cm) • Thermal runaway is small ($\Delta T = 10.5$ K at 80 s)
Recommendations		• SiC-metallic support is the optimal heating strategy for w/o emulsions with all ranges of water fractions (ϕ) during R_1 mode • Metallic and Alumina-metallic supports are suitable strategies for w/o samples with larger processing thickness corresponding to R_2 mode for all ranges of water fractions (ϕ)	

modes. For both o/w and w/o emulsions, it is observed that microwave power absorption is enhanced in presence of metallic and composite supports and average power is larger than that with individual ceramic support during both the significant resonance modes R_1 and R_2. A detailed mathematical analysis on individual traveling waves has been carried out to study the role of specific support assembly (ceramic and/or metallic) on spatial power and temperature distributions within emulsion samples corresponding to both R_1 and R_2 modes. Finally, the suitability of an efficient microwave heating strategy has been illustrated based on temperature difference (ΔT) and average temperature ($\overline{T}$) vs time plot for both o/w and w/o emulsion samples.

Table 2 summarizes microwave heating characteristics for o/w emulsions corresponding to efficient heating strategies such as metallic support, Alumina-metallic support and SiC-metallic support. Choice of suitable heating strategy corresponding to any specific resonance mode (R_1 or R_2) is a strong function of heating rates, thermal runaway, processing thickness and fraction of the dispersed phase (ϕ). It is interesting to note that, any suitable choice is ultimately judged based on thermal runaway and heating rate for specific emulsion sample. It is observed that, SiC-metallic composite support corresponds to smaller thermal runaway with moderately large heating rates for o/w emulsion samples with larger oil fractions ($\phi \geqslant 0.45$) whereas metallic and Alumina-metallic composite supports correspond to larger heating rates with smaller thermal runaway for o/w samples with smaller oil fractions ($\phi = 0.3$) during R_1 mode. Therefore, SiC-metallic composite support may be recommended as an optimal heating strategy for o/w samples with larger oil fractions ($\phi \geqslant 0.45$) and metallic and Alumina-metallic composite supports may be suitable choices for samples with smaller oil fractions ($\phi = 0.3$). It is also observed that, metallic and Alumina-metallic composite supports correspond to reasonably large heating rates with very small thermal runaway for o/w samples with all ranges of oil fractions (ϕ) during R_2 mode which corresponds to larger processing thickness. Hence, metallic and Alumina-metallic composite supports are suitable choices for processing of o/w emulsions with larger sample dimensions.

It is interesting to observe that, SiC-metallic composite support corresponds to smaller thermal runaway with optimal heating rates for w/o emulsion samples with all ranges of water fractions (ϕ) during R_1 mode (as seen in Table 3). Therefore, it may be recommended as an optimal heating strategy for w/o samples with all ϕ values. It may be noted that, thermal runaway is small for w/o samples with all ranges of water fractions during R_2 mode, for metallic and both composite supports. Hence, due to slightly larger heating rates, metallic and Alumina-metallic composite supports may be chosen as the suitable strategies for processing of w/o emulsions with larger sample dimensions corresponding to R_2 mode.

Based on the overall scenarios, it is observed that either metallic and Alumina-metallic supports or SiC-metallic support may be useful to achieve optimal heating rates and microwave processing can be carried out either at R_1 or R_2 mode depending upon the specific requirements of smaller thermal runaway and larger processing thickness for various o/w and w/o emulsion samples. Tables 2 and 3 may provide some useful guidelines for optimal microwave processing of o/w and w/o emulsions supported with ceramic and/or metallic plates in a single mode waveguide operated with uniform plane waves.

Acknowledgement

Authors would like to thank anonymous reviewers for critical comments which improved the quality of the manuscript.

References

[1] H.Y. Kim, H.C. Kim, V.V. Levdansky, V.G. Leitsina, J. Smolik, Chemical deposition of substance from gas phase in nonisothermal channels, Int. J. Heat Mass Transfer 43 (2000) 3877–3882.
[2] J. Zhu, A.V. Kuznetsov, K.P. Sandeep, Mathematical modeling of continuous flow microwave heating of liquids (effects of dielectric properties and design parameters), Int. J. Therm. Sci. 46 (2007) 328–341.
[3] D. Burfoot, C.J. Railton, A.M. Foster, S.R. Reavell, Modelling the pasteurization of prepared meals with microwaves at 896 MHz, J. Food Eng. 30 (1996) 117–133.
[4] T. Basak, Analysis of microwave propagation for multilayered material processing: lambert's law versus exact solution, Ind. Eng. Chem. Res. 43 (2004) 7671–7675.
[5] Q.O. Zhang, T.H. Jackson, A. Ungan, Numerical modeling of microwave induced natural convection, Int. J. Heat Mass Transfer 43 (2000) 2141–2154.
[6] Q. Zhang, T.H. Jackson, A. Ungan, D. Gao, Numerical modeling of continuous hybrid heating of cryopreserved tissue, Int. J. Heat Mass Transfer 42 (1999) 395–403.
[7] A. Kelen, S. Ress, T. Nagy, E. Pallai-Varsanyi, K. Pintye-Hodi, "3D layered thermography" method to map the temperature distribution of a free flowing bulk in case of microwave drying, Int. J. Heat Mass Transfer 49 (2006) 1015–1021.
[8] Z. Tao, H.W. Wu, G.H. Chen, H.W. Deng, Numerical simulation of conjugate heat and mass transfer process within cylindrical porous media with

cylindrical dielectric cores in microwave-freeze drying, Int. J. Heat Mass Transfer 48 (2005) 561–572.
[9] P. Salagnac, P. Glouannec, D. Lecharpentier, Numerical modeling of heat and mass transfer in porous medium during combined hot air, infrared and microwave drying, Int. J. Heat Mass Transfer 47 (2004) 4479–4489.
[10] P. Rattanadecho, Theoretical and experimental investigation of microwave thawing of frozen layer using a microwave oven (effects of layered configuration and layer thickness), Int. J. Heat Mass Transfer 47 (2004) 937–945.
[11] C.S. Fang, P.M.C. Lai, Microwave-heating and separation of water-in-oil emulsions, J. Microwave Power Electromagnetic Energy 30 (1995) 46–57.
[12] C.C. Chan, Y.C. Chen, Demulsification of w/o emulsions by microwave radiation, Separ. Sci. Technol. 37 (2002) 3407–3420.
[13] L.X. Xia, S.W. Lu, G.Y. Cao, Stability and demulsification of emulsions stabilized by asphaltenes or resins, J. Colloid Interf. Sci. 271 (2004) 504–506.
[14] A. Chatterjee, T. Basak, K.G. Ayappa, Analysis of microwave sintering of ceramics, AIChE J. 44 (1998) 2302–2311.
[15] Q. Pang, J.X. Shi, Y. Liu, D.S. Xing, M.L. Gong, N.S. Xu, A novel approach for preparation of $Y_2O_3 : Eu^{3+}$ nanoparticles by microemulsion-microwave heating, Mater. Sci. Eng. -B 103 (2003) 57–61.
[16] K.G. Ayappa, H.T. Davis, E.A. Davis, J. Gordon, Analysis of microwave heating of materials with temperature-dependent properties, AIChE J. 37 (1991) 313–322.
[17] K.G. Ayappa, H.T. Davis, G. Crapiste, E.A. Davis, J. Gordon, Microwave heating: an evaluation of power formulations, Chem. Eng. Sci. 46 (1991) 1005–1016.
[18] K.G. Ayappa, H.T. Davis, E.A. Davis, J. Gordon, Two-dimensional finite element analysis of microwave heating, AIChE J. 38 (1992) 1577–1592.
[19] K.G. Ayappa, H.T. Davis, S.A. Barringer, E.A. Davis, Resonant microwave power absorption in slabs and cylinders, AIChE J. 43 (1997) 615–624.
[20] K.G. Ayappa, Resonant microwave power absorption in slabs, J. Microwave Power Electromagnetic Energy 34 (1999) 33–41.
[21] T. Basak, K.G. Ayappa, Analysis of microwave thawing of slabs with effective heat capacity method, AIChE J. 43 (1997) 1662–1674.
[22] T. Basak, K.G. Ayappa, Influence of internal convection during microwave thawing of cylinders, AIChE J. 47 (2001) 835–850.
[23] T. Basak, K.G. Ayappa, Role of length scales on microwave thawing dynamics in 2D cylinders, Int. J. Heat Mass Transfer 45 (2002) 4543–4559.
[24] T. Basak, Analysis of resonances during microwave thawing of slabs, Int. J. Heat Mass Transfer 46 (2003) 4279–4301.
[25] S.A. Barringer, K.G. Ayappa, E.A. Davis, H.T.J. Gordon, Power absorption during microwave-heating of emulsions and layered systems, J. Food Sci. 60 (1995) 1132–1136.
[26] T. Basak, Role of resonances on microwave heating of oil–water emulsions, AIChE J. 50 (2004) 2659–2675.
[27] T. Basak, A.S. Priya, Role of ceramic supports on microwave heating of materials. J. Appl. Phys. 97 (2005) (Art. No. 083537).
[28] R. Pal, Techniques for measuring the composition (oil and water-content) of emulsions - a state-of-the-art review, Colloids Surfaces A 84 (1994) 141–193.
[29] U. Erle, M. Regier, C. Persch, H. Schubert, Dielectric properties of emulsions and suspensions: mixture equations and measurement comparisons, J. Microwave Power Electromagnetic Energy 35 (2000) 185–190.
[30] J.N. Reddy, An Introduction to the Finite Element Method, McGraw-Hill, New York, 1993.